Newmark sliding block model for pile-reinforced slopes under earthquake loading

Al-Defae, A. H.; Knappett, J. A.

Published in:
Soil Dynamics and Earthquake Engineering

DOI:
10.1016/j.soildyn.2015.04.013

Publication date:
2015

Elsevier Editorial System(tm) for Soil Dynamics and Earthquake Engineering
Manuscript Draft

Manuscript Number: SOILDYN-D-14-00245R2

Title: Newmark sliding block model for pile-reinforced slopes under earthquake loading

Article Type: Research Paper

Keywords: Slope stability; Earthquakes; Centrifuge models; Piles; Sands; Embankments.

Corresponding Author: Dr. Jonathan Knappett, MA MEng PhD

Corresponding Author's Institution: University of Dundee

First Author: Asad H Al-Defae, BSc PhD

Order of Authors: Asad H Al-Defae, BSc PhD; Jonathan Knappett, MA MEng PhD

Cover Letter

School of Engineering, Physics and Mathematics

14th April, 2015

To the Editor in Chief,

Re: Submission of revised manuscript for publication in Soil Dynamics and Earthquake Engineering:

"Newmark sliding block model for pile-reinforced slopes under earthquake loading" (Revision 2)

My co-author and I hereby submit the above named revised manuscript for publication in Soil Dynamics and Earthquake Engineering as a full technical paper. We have included a full response to the reviewers' additional minor comments.

We hereby confirm that the paper is entirely original and is not under consideration by any other journal.

Should you require any further information, please do not hesitate to contact me on j.a.knappett@dundee.ac.uk.

Yours sincerely,

Jonathan Knappett (Corresponding author)
Senior Lecturer

Reviewer #1: Responses to my review comments on the original paper are accepted. The following comments refer to the Rev 1 of the paper:

1. Line 37: Suggest replacing the word "conglomerate" with "combined" because I suspect that a conglomerate soil-pile interaction model will be interpreted by some as assessing soil-pile interaction in a conglomerate soil. I realize that I used this term in my initial review comments but in the paper itself I think it is too risky given the usual use of this term in the geological context in our profession.

> ***We have replaced "conglomerate" with "combined" as suggested.***

2. Line 74: Suggest replacing the word "complimentary" with "more".

> ***We thank the reviewer for spotting this misspelling. We had meant "complementary" as we believe the simplified model would be useful when combined as a two stage analysis with Newmark first, followed by FEM, as outlined in lines 79-81. We have therefore changed the word to "complementary".***

3. Line 193: Two relationships are presented for Equation (7) but only one applies (the second one) - need to delete the first relationship given for p.

> ***We think this was due to a hidden equation object (it does not appear in our word file, but becomes visible when converted to pdf). We believe this has now been corrected.***

4. Line 194: Delete the letter "p" preceding "Pi".

> ***Corrected as suggested.***

5. Line 200: Two relationships are presented for Equation (8) but only one applies (the second one) - need to delete the first relationship given for pult.

> ***We think this was due to a hidden equation object (it does not appear in our word file, but becomes visible when converted to pdf). We believe this has now been corrected.***

6. Line 201: Delete the letter "d" preceding "Deq".

> ***Corrected as suggested.***

7. Line 512: Suggest replacing the word "conglomerate" with "combined" as per my reasoning given in Comment #1.

> ***We have replaced "conglomerate" with "combined" as suggested.***

Highlights:

- A sliding block method incorporating strain-dependent pile resistance is presented.
- Discontinuity Layout Optimisation (DLO) was used to find slip plane location.
- The sliding block method was validated against centrifuge test data.
- Slope deformations and maximum pile moments were well predicted.
- The method was also validated for multiple sequential motions (aftershocks).

Newmark sliding block model for pile-reinforced slopes under earthquake loading

Al-Defae, A.H.[1] and Knappett, J.A.[2]*

[1] University of Dundee, Dundee, UK & Wasit University, Iraq;

[2] University of Dundee, Dundee, UK.

Original submission: 27 June 2014

Revision 1: 05 January 2015

Revision 2: 14 April 2015

Keywords: Slope stability; Earthquakes; Centrifuge models; Piles; Sands; Embankments.

No. of words: 6,109 (excl. abstract, references and acknowledgements)

No: of tables: 1

No. of figures: 20

*Corresponding author: Dr J. A. Knappett
Senior Lecturer
Division of Civil Engineering
University of Dundee
Nethergate
Dundee
DD1 4HN
T: +44-1382-384345
F: +44-1382-344816
E: j.a.knappett@dundee.ac.uk

Abstract

Recent studies have demonstrated that the use of a discretely-spaced row of piles can be effective in reducing the deformations of slopes in earthquakes. In this paper, an approximate strain-dependant Newmark sliding-block procedure for pile-reinforced slopes has been developed, for use in analysis and design of the piling scheme, and the model is validated against centrifuge test data. The interaction of the pile within the slipping soil was idealised using a non-linear elasto-plastic (*P*-*y*) model, while the interaction within the underlying stable soil was modelled using an elastic response model in which (degraded) soil stiffness is selected for an appropriate amount of shear strain. This combined soil-pile interaction model was incorporated into the improved Newmark methodology for unreinforced slopes presented by Al-defae et al. [1], so that the final method additionally incorporates strain-dependent geometric hardening (slope re-grading). When combined with the strain-dependent pile resistance, the method is therefore applicable to analysis of both the mainshock and subsequent aftershocks acting on the deformed slope. It was observed that the single pile resistance is mobilised rapidly at the start of a strong earthquake and that this and the permanent slope deformation are therefore strongly influenced by pile stiffness properties, pile spacing and the depth of the slip surface. The model shows good agreement with the centrifuge test data in terms of the prediction of permanent deformation at the crest of the slope (important in design for selecting an appropriate pile layout/spacing i.e. *S/B*) and in terms of the maximum permanent bending moments induced in the piles (important for appropriate structural detailing of the piles), so long as the slip surface depth can be accurately predicted. A method for doing this, based on limit analysis, is also presented and validated.

Keywords: Slopes, Piles, Sand, Analytical modelling, Centrifuge modelling,

1. Introduction

The technique of slope stabilisation by piling is widely used by geotechnical engineers to utilise the bending response of the pile to stabilise the sliding mass by coupling this to stronger stable strata below. The piling would typically be installed as a discretely-spaced pile row running along the length of the slope at a centre-to-centre spacing, *S*, with a sufficient length to allow them to pass through the unstable slipping soil mass and become anchored in the underlying stable soil. In the pre-failure stage the piles promote arching of stresses between adjacent piles which improves stability [2, 3]. If the soil mass slips (the piles being designed to remain elastic), the ground movements generate relative soil-pile displacement, which in turn leads to the mobilisation of lateral earth pressures along the piles, and additional resistance due to the subsequent pile bending.

In the analysis and design of such piling schemes, it is important to be able to determine (i) the reductions in seismic displacement for a given pile arrangement (e.g. normalised spacing *S/B*, where *B* is the pile width or diameter) so that the piling can be designed to give the required improvement to the geotechnical performance (i.e. reduction in slip); and (ii) internal forces (e.g. bending moments) within the piles, so that they can be structurally detailed. Analytical solutions have been developed for the analysis of pile-slope systems under static loads (e.g. [4 – 6]). Kourkoulis et al. [7] have demonstrated the use of Finite Element (FE) modelling for analysing the performance of piled slopes under seismic loading, but it would be useful in preliminary design phases to have a complementary simple model which can provide the required response parameters rapidly without requiring the use of finite element software. Such a tool would be useful for (i) conducting large parametric studies; (ii) use in performance-based earthquake engineering where statistical approaches and Monte-Carlo simulation may be necessary; and (iii) in refining the design before more detailed FE modelling is conducted to verify final performance, thereby potentially reducing the amount of FE modelling which is required.

In this paper, a simplified approximate soil-pile interaction (SPI) model for determining mobilised pile resistance with soil slip is formulated for piles passing through a slipping soil mass and anchored into stable soil beneath. This is then incorporated within a Newmark sliding block analysis [8, 9] through an enhanced yield acceleration considering the forces (including mobilised pile resistance) acting on the slipping soil mass. In this case, an improved Newmark analysis methodology, developed recently by Al-defae et al. [1], is used with this yield acceleration. This methodology additionally incorporates strain-dependent geometric hardening (slope re-grading) through updating the instantaneous slope angle in each time step. As the soil-pile resistance and slope geometry is tracked throughout the analysis as a function of soil slip (i.e. strain), the new model is implicitly suitable for also estimating performance in subsequent accompanying aftershocks which may occur on an already-damaged slope (i.e. before it has been repaired). The model developed is validated against centrifuge test data for pile-reinforced sandy slopes reported previously by Al-defae and Knappett [10].

2. Sliding block procedure for pile-reinforced slopes

2.1 Formulation

The limit equilibrium formulation for the yield acceleration of an infinite slope developed by Al-defae et al. [1], which includes strain-dependent geometric hardening of the slope, is here modified to incorporate the additional component of resistance to sliding provided by the piles. For slip of a moving mass of soil of length *L*, width *S*, unit weight *γ* and with a slip plane depth of z_{slip} beneath the slope surface, the applied downslope shear stress from Figure 1 is:

$$\tau_{applied} = \gamma z_{slip} \sin\beta \cos\beta + k_h \gamma z_{slip} \cos^2\beta \qquad (1)$$

where the first term relates to the static shear stress due to the ground slope, and the second term relates to the additional peak dynamic downslope shear stress induced by the earthquake shaking. The total shear resistance to this applied shear stress is given by:

$$\begin{aligned}\tau_{ult} &= c' + \sigma' \tan\phi' + \frac{P}{LS}\cos\beta \\ &= c' + \left(\gamma z_{slip}\cos^2\beta - k_h \gamma z_{slip}\sin\beta\cos\beta - u\right)\tan\phi' + \frac{P}{LS}\cos\beta\end{aligned} \tag{2}$$

where P is the horizontal shear resistance force provided by a single pile, determined from the soil-pile interaction model presented in Section 3. The soil yields when $\tau_{\text{applied}} = \tau_{\text{ult}}$. The value of k_h at which this occurs (i.e. the yield acceleration, k_{hy}) can be determined from Equations (1) and (2) as:

$$k_{hy} = \frac{c' + \left(\gamma z_{slip}\cos^2\beta - u\right)\tan\phi' - \gamma z_{slip}\sin\beta\cos\beta + \dfrac{P}{LS}\cos\beta}{\gamma z_{slip}\cos^2\beta + \gamma z_{slip}\sin\beta\cos\beta\tan\phi'} \tag{3}$$

In Equation (3), u', β, L and P are functions of shear strain (ε_s) on the shear plane due to slope displacement. Al-defae et al. [1] showed that the strain softening model of Matasovic et al. [9] can be used to describe $u'(\varepsilon_s)$. A simple relationship was then developed to describe the geometric effect of an increment of slip in reducing the slope angle (β), which is shown in Figure 2. Numerically within the Newmark sliding block method, the slope angle is updated for step i+1 based on the slope angle (β_i) and the amount of slope-parallel slip (d_i), both from the previous step, using:

$$\beta_{i+1} = \tan^{-1}\left(\frac{H_i - d_i\sin\beta_i}{H_i\cot\beta_i + d_i\cos\beta_i}\right) \tag{4}$$

For the initial time step (i = 0): $d_0 = 0$, $H_i = H$ and $\beta_i = \beta_0$, as in [1]. When considering the relative contribution of a pile and the soil shear strength to the total resistance, the instantaneous slip-plane length (L_i) is also required, which is related to the instantaneous slope angle by:

$$L_i = \frac{H_i}{\sin \beta_i} \quad (5)$$

The pile resistance (P) as a function of strain (soil slip) depends on a number of parameters describing the relative soil-pile stiffness and relative soil-pile strength. Clearly, in the initial stages of the analysis before any slip has taken place, the net additional resistance from the piles is zero. As the soil slips, the relative displacement between the soil and the pile increases, providing a progressively larger resistance to slip. Eventually, the resistance from the pile will reach a maximum limiting value when either the soil yields around the pile, or the pile yields structurally, whichever occurs first. In designing an arrangement of slope stabilising piles, it will be desirable for the piles to remain elastic such that the soil fails before the piles and the piled slope therefore has its maximum possible resistance to sliding. This approach has the added benefit that once fully mobilised, the maximum soil-pile resistance will remain at this maximum level for subsequent earthquakes, without the piles becoming extensively damaged.

As the soil starts to slip, P will increase, while β will reduce, due to the effects described above. Both changes will result in progressive hardening of the slope response via an increase in the yield acceleration (Equation (3)). Even once the piles are providing their maximum resistance, the slope response will continue to be reduced compared to the unreinforced case due to (i) the constant value of P in Equation (3), so long as the soil or pile are yielding in a ductile way, and (ii) the continued geometric hardening. By fully incorporating the effects of strain within the model, the behaviour of a seismically damaged slope during subsequent earthquakes/aftershocks can be determined by starting such an analysis from the initial conditions (pile resistance, amount of slip, re-graded slope angle) obtained at the end of the previous ground motion, as presented for unreinforced slopes in [1].

2.2 Assumptions and simplifications

For small to moderate earthquakes whose peak ground acceleration magnitude is close to (but larger than) k_{hy} and which will therefore have only a limited amount of slip, strain-softening behaviour [9] can have a dramatic effect on computed slope displacements, with k_{hy} potentially changing continuously throughout the earthquake as ϕ' softens. In larger earthquakes, where a single cycle causes sufficient slip/strain to reach critical state conditions, then the strain softening model is likely to predict only a marginally smaller slip compared to a standard (strain-hardening) analysis using a constant $\phi' = \phi'_{cs}$ [1]. Therefore, a constant friction angle is used throughout the model in this paper. Michalowski and Shi [11] showed that the deformation in sandy layers can be represented using a non-associative flow rule and that an associative flow rule (normality principle) does not accurately describe deformation in granular soil. Thus, in this paper, a generalised non-associative condition is assumed, which is incorporated using a modified friction angle ϕ^* following [12]:

$$\tan\phi^* = \frac{\cos\psi'\cos\phi'_{pk}}{1-\sin\psi'\sin\phi'_{pk}}\tan\phi'_{pk} \qquad (6)$$

where ϕ'_{pk} is the peak friction angle and ψ' is the angle of dilation.

It is also assumed, as in [1], that once the slope has deformed to a new, smaller value of β the failure mechanism will continue to be of the infinite type, with a new slip surface forming parallel to the new slope surface. This allows the model to be used even for the case of large total slope movements (such as may accrue during a series of strong aftershocks) as the displacement increment in each individual time step remains small, and therefore the instantaneous failure mechanism can be represented by Figure 2 for small displacements.

3. Soil-pile interaction (SPI) model

In this section, the relationship between the instantaneous amount of soil slip, y_{si} (= Σd_i), and the corresponding pile resistance, P_i, is developed. This relationship, hereafter termed the SPI model, will also enable the peak bending moments to subsequently be derived within the piles, so that they can be appropriately detailed. Given that, as described previously, the aim in design will be to ensure the piles remain undamaged, it can be assumed that the soil in the slipping mass will yield around the piles. The interaction in this zone of soil is here described using a single non-linear elasto-plastic *P-y* curve ('spring') which describes the force applied on the pile by the slipping soil (and vice-versa), P_i, as a function of the relative displacement between the soil and the pile ($y_{si} - y_{pi}$) at the point of resultant load application. The part of the pile within the stable soil is modelled using a linearised elastic response model describing the response of the pile at the point of load application (y_{pi}) under the applied load P_i. This simplified conglomerate approach is shown schematically in Figure 3.

3.1 Soil-pile interaction in slipping soil

P-y curves are popular for describing the non-linear relationship between soil resistance and relative soil-pile deformation. O'Neill and Murchison [13] developed a procedure which was subsequently adopted by the American Petroleum Institute (API) to determine the load-deflection relationship (*P-y* curve) in sands. This method is used herein within the slipping soil. The *P-y* curve in this procedure consists of an hyperbolic tangent function to represent the non-linearity in the response. This relationship is written as:

$$P_i = Ap_u \tanh\left[\frac{kz_{slip}}{Ap_u}\left(y_{si} - y_{pi}\right)\right] z_{slip} \qquad (7)$$

where P_i is the resultant soil-pile reaction over the length of the pile within the slipping soil mass (i.e. over a section of length z_{slip}), p_u is the ultimate soil resistance per unit length of the pile (see below) at soil yield, y_{si} is the cumulative soil slip, y_{pi} is the lateral pile displacement at the location of the *P-y* curve, k is the initial modulus of subgrade reaction and A is a factor to account for cyclic loading (A = 0.9 for cyclic loading; A = 1.0 for monotonic loading). The ultimate capacity per unit length, p_u, is calculated as:

$$p_u = \left(C_1 z_{slip} + C_2 D_{eq}\right)\gamma' z_{slip} \tag{8}$$

where D_{eq} is the equivalent pile diameter (for a square pile this is assumed to be equal to the pile width, i.e. $D_{eq} = B$) and γ' is the effective unit weight of the soil (= $\gamma - \gamma_w$). The coefficients C_1 and C_2 and the initial subgrade reaction k are determined as a function of the angle of internal friction as outlined in [14] and summarised in Figure 4.

3.2 Soil-pile interaction in stable soil

In the stable soil, the soil is initially assumed to remain elastic, with the relationship between applied load and pile displacement presented by Randolph [15]. Its implementation here is shown schematically in Figure 5. It is assumed that the lateral pressure acting on the pile within the unstable soil increases approximately linearly with depth, so that the resultant horizontal force on the pile from the slipping soil (i.e. the *P-y* spring force) acts at a depth of $0.67z_{slip}$ below the top of the pile. This means that the pile length within the stable soil is treated as a partially embedded pile acted upon by a resultant horizontal force (= P_i) and moment (= $P_i \times 0.33\, z_{slip}$) acting at the level of the shear plane. The resulting relationship between P_i and y_{pi} is given by:

$$P_i = \frac{\rho_c G_c L_c}{\cos\beta_i \left(\dfrac{E_p}{G_c}\right)^{\frac{1}{7}} \left[0.54 + 0.40\dfrac{z_{slip}}{L_c}\right]} y_{pi} \tag{9}$$

where:

$$E_p = \frac{64EI}{\pi D_{eq}^4} \tag{10}$$

$$L_c = D_{eq}\left(\frac{E_p}{G_c}\right)^{\frac{2}{7}} \quad (11)$$

$$G_c = \overline{G}_{Lc}(1 + 0.75\nu) \quad (12)$$

$$\rho_c = \frac{G(z_{slip} + L_c/4)}{\overline{G}_{Lc}} \quad (13)$$

The parameter $\overline{G}_{Lc}$ is the median value of the operative shear modulus over the critical length (L_c), i.e. the value of G at a depth of $L_c/2$, and ρ_c is an homogeneity factor describing the variation of G with depth. The method can therefore account for (linear) variation of soil shear modulus with depth within the stable soil, and pile sections of any bending stiffness and cross-section EI (through use of an equivalent elastic circular pile of Young's Modulus E_p, Equation 10).

The key modification made to this existing model in this paper is that the 'operative' shear modulus (G) is reduced to account for the effects of cyclic shearing in the free-field (which is here assumed to also approximate the cyclic effects in the near-field soil). The analytical estimation of this G-z relationship is described in Section 3.3. To use Equations (11) – (13) some iteration is required due to the inter-relationships between L_c and G_c. In practice an initial value of L_c is assumed and used to determine G_c. This value of G_c is then used in Equation (11) to calculate an improved estimate of L_c. This changes G_c (c.f. Figure 5). The procedure is repeated until the values of G_c and L_c are consistent with each other.

3.3 Estimation of operative shear modulus in stable soil

The 'operative' shear modulus (G-z relationship) required for the 'stable' part of the SPI model can be determined based on the initial small-strain shear modulus (G_o) for the soil before cyclic loading (from Hardin and Drnevich [16] – Equation 14) and the variation of

RMS average cyclic shear stress (τ_{av}) and cyclic shear strain ($\varepsilon_{s,cyc}$) with depth during the earthquake (Equation 15):

$$G_o = 100\left[\frac{(3-e)^2}{1+e}\right](p'_0)^{0.5} \tag{14}$$

$$\frac{G}{G_o} = \frac{\tau_{av}}{G_o \varepsilon_{s,cyc}} \tag{15}$$

where $p'_0 = (1 + 2K_0)\sigma'_{v0}/3$ is the initial mean confining stress (K_0 being the coefficient of lateral earth pressure) and e is the void ratio. The cyclic shear stress is estimated using an equation proposed by Seed and Idriss [17] where the RMS average cyclic shear stress caused by earthquake was estimated as approximately 0.65 times the peak shear stress:

$$\tau_{av} = 0.65\left(\frac{a_{\max}}{g}\right)\sigma_{v0} r_d \tag{16}$$

where $a_{\max}$ is the peak ground acceleration at the soil surface, g is the acceleration due to gravity, σ_{v0} is the total overburden stress, and r_d is a stress reduction coefficient which is here determined following [18]:

$$r_d = e^{[\alpha_1(z)+\alpha_2(z).M_w]} \tag{17}$$

where M_w is the earthquake magnitude, z is the depth below ground surface in meters and:

$$\alpha_1 = -1.012 - 1.126\sin\left(\frac{z}{11.73} + 5.133\right) \tag{18}$$

$$\alpha_2 = 0.106 + 0.118\sin\left(\frac{z}{11.28} + 5.142\right) \tag{19}$$

The cyclic shear strain ($\varepsilon_{s,cyc}$) is estimated using Equation (20) as proposed by Pradel [19]:

$$\varepsilon_{s,cyc}\ (\%) = \left\{ \frac{1 + a.e^{(b.\tau_{av.}/G_0)}}{1+a} \right\} \frac{\tau_{av.}}{G_0} \times 100 \qquad (20)$$

where

$$a = 0.0389\left(\frac{p_0'}{p_a}\right) + 0.124 \qquad (21)$$

$$b = 6400\left(\frac{p_0'}{p_a}\right)^{-0.6} \qquad (22)$$

In Equations (21) – (22) p_a is atmospheric pressure (100 kPa).

3.4 Pile spacing effects (pile 'shadowing') and local non-linearity in stable soil

When using piles in a closely spaced pile row, the zones of soil into which the piles displace relative to the soil may overlap, resulting in a reduction in the resistive force available due to 'shadowing' [3]. This is accounted for in the present analysis by applying the *p*-multiplier concept, i.e. by multiplying the values of *P* in the SPI model by a factor p_m between 0 – 1, dependent on the pile spacing. Previously proposed *p*-multipliers for circular piles are summarised in Figure 6. A simple bi-linear approximate relationship was inferred from this data for use within the SPI model, having a cut-off spacing of 5*B*, given by:

$$p_m = \begin{cases} 0.235\dfrac{S}{B} - 0.168 & \dfrac{S}{B} \le 5.0 \\ 1.0 & \dfrac{S}{B} \ge 5.0 \end{cases} \qquad (23)$$

It is here assumed that Equation (23) applies to both circular piles of diameter *B* and square piles of side *B* (as previously assumed in Equations (8), (10 and (11)).

While the slipping soil mass incorporates elasto-plastic behaviour through the *P-y* approach (Equation 7), the stable soil model presented in Section 3.2 is based on a purely elastic soil response to relative soil-pile movement (albeit in a soil medium which has reduced operative stiffness due to shaking – Section 3.3). In reality, however, there may be a modest amount of non-linearity in the stable mass just below the location of the slip plane where the relative soil-pile deformations due to pile deflection will be larger [21]. To maintain the simplicity of the method, this effect is incorporated through a further reduction in soil stiffness used in Equations (9) – (13). Based on data from full-scale pile tests (Figure 7 shows data for piles in sand appropriate for this study after [22]) a simple empirical relationship can be determined for a reduction factor on elastic pile stiffness as a function of (normalised) pile displacement:

$$g_m = \begin{cases} 1.0 & \dfrac{y_{pi}}{B} \le 0.004 \\ 6.40\times10^{-2}\left(\dfrac{y_{pi}}{B}\right)^{-0.5} & \dfrac{y_{pi}}{B} \ge 0.004 \end{cases} \tag{24}$$

3.4 Combined SPI model

For use within the sliding block method, i.e. for determining the instantaneous value of P_i in Equation (3), a direct relationship between P_i and slope slip y_{si} is desirable, so that the slip computed from the previous step can be used to obtain the current pile resistance force. This can be achieved by following the following procedure:

1. Estimate the operative shear modulus within the stable soil (Section 3.3) and use this to determine G_c, ρ_c and L_c.
2. Substitute Equation (9) into Equation (7) for the unknown pile displacement y_{pi}.
3. The resulting (non-linear) closed-form expression can then be used to evaluate P_i over a fine grid of y_{si} values using the values of G_c, ρ_c and L_c from step (1), and these values of P_i reduced by p_m to account for the pile spacing.
4. Values of y_{pi} compatible with the P_i, y_{si} pairs can then be evaluated using either Equation (7) or Equation (9) and used to determine stiffness multipliers g_m.

5. The stiffness G_c is reduced by g_m and reduced values of P_i are evaluated over the same grid of y_{si} values.

The result of this procedure is a unique P_i-y_{si} curve which can be used at a particular time step in a sliding block analysis to evaluate the current resistance force based on the current accumulated soil slip from the previous step. This force is then used in Equation (3) to evaluate the current value of k_{hy} for determining slope deformation via Newmark analysis. A flowchart, showing the complete procedure is shown in Figure 8.

3.5 Determination of bending moment profile in piles

Once the sliding-block analysis has been completed, the variation of P with time will have been determined as an integral part of the analysis. Once this instantaneous load is known, it is relatively simple to estimate the bending moments within the pile as they are proportional to P while the pile remains elastic. Randolph [15], as cited in Fleming et al. [23], present normalised bending moment profiles for partially embedded piles (which, following the previous analogy, apply below the slip plane in this case) for the cases of moment-only loading and shear-only loading. If the pile remains elastic, the principal of superposition can be used to combine the effects of the shear force (= P_i) and moment (= $P_i \times 0.33z_{slip}$) acting at the location of the slip plane depth. Above the slip plane (i.e. within the slipping soil) the bending moments are assumed to reduce linearly from the value at the slip plane to zero at the ground surface (consistent with the lateral bearing capacity of the soil increasing linearly with the depth and all of the soil within this zone being at yield).

Normalised moment curves ($M_i / P_i L_c$) for different slip plane depths have been created as a function of normalised depth below the slip plane $\left(z - z_{slip}\right)/ L_c$ and these are shown in Figure 9 for ρ_c = 1.0 i.e. for G increasing linearly with depth. As the value of β_i reduces with slip, once the pile has reached its ultimate value of P (soil slip around the pile) there can be further increase in the induced moments due to re-grading.

4. Validation of Newmark method for piled slopes against centrifuge data

4.1 Centrifuge modelling

Dynamic centrifuge testing was conducted using the 3.5 m diameter beam centrifuge and servo-hydraulic earthquake simulator (EQS) at the University of Dundee. The modelling and observations from these tests are described in detail in [10]; only a brief summary is given here. All subsequent properties are reported at prototype scale.

The results of six tests from this previously reported programme are utilised herein for validation of the Newmark model, representing identical 1:2 slopes ($\beta_0 \approx 28°$) at 1:50 scale in dry HST95 sand and tested at 50-g. The sand was pluviated in air using a slot pluviator into an Equivalent Shear Beam (ESB) container having flexible walls, the construction of which is described in [24]. The slopes were prepared at a relative density of D_r = 55 – 60% (the range accounts for the accuracy in being able to measure and replicate D_r), 8 m tall from toe to crest and were underlain by a further 6 m of sand at the same relative density. Table 1 shows a summary of the test properties, while the arrangement and instrumentation of the slope models are shown in Figure 10.

Where piles were used these all had a square cross-section with B = 0.5 and an 'elastic' section with a high moment capacity (M_{ult}), fabricated from aluminium alloy as described in [10]. Two of these piles in each test were instrumented to measure bending moments along the length (for comparison to the assumed distributions shown in Figure 9). The bending stiffness of the piles was EI = 50.4 MNm^2 and M_{ult} = 3750 kNm

The test programme also included the use of two different strong earthquake motions to allow an initial assessment of the model's sensitivity to shaking characteristics. Four tests used a motion recorded at Station TCU072 during the M_w = 7.6 Chi-Chi Earthquake in 1999, having a peak ground acceleration (PGA) = 0.41-g, while two tests (AA17 and AA16, see Table 1) used a motion recorded at the Nishi-Akashi recording station in the M_w = 6.9 Kobe earthquake in 1995 (PGA = 0.43-g). The characteristics of these motions are described in

[1]. In each case four nominally identical motions were applied to each model in sequence to allow the performance in strong aftershocks to be validated.

4.2 SPI model for parameters used in the centrifuge tests

Figure 11 shows the variation of initial shear modulus (G_o), operative shear modulus (G) calculated using Equation (15) and the measured shear modulus in the free-field from the centrifuge test data. The latter was derived from the time-acceleration histories from instruments 6, 10 and 15 in Figure 10, which were located at the middle of the slope and along the centreline of the container (midway between the two central piles), following the method outlined by Brennan et al. [25]. Figure 12 shows time-shear stress, time-shear strain and a shear stress-shear strain cycle at peak cyclic shear strain from centrifuge test AA14 as an example. Some differences are observed between the operative and measured shear moduli in Figure 11, but the approximate procedure described in Section 3.3 appears to provide a rational basis for making a reasonable estimation of the operative shear modulus for use in the SPI model.

Figure 13 shows the P-y_s curves for pile resistance, using soil properties for the centrifuge tests (υ'_{pk} = 40°; ψ' = 10°; υ^* = 35° - see [1]). At S/B = 7.0 there is no shadowing effect (p_m = 1.0 from Equation (24)) while the curves are reduced in magnitude at S/B = 4.7 and 3.5. It is clear that once the soil slips by a relatively small amount (10 mm in this case) the pile resistance reaches a maximum value consistent with the unstable soil yielding around the piles. Expressing this displacement in terms of the pile size, 0.015B, the value is consistent with the lower limit of previous findings for the static case [26, 27] which suggest that the ultimate pile resistance is mobilised within the range 0.015D_{eq} to 0.025D_{eq}.

4.3 Analysis procedure

To use the sliding block method developed in the previous sections, it is necessary to know the slip plane depth, z_{slip}. In the centrifuge tests z_{slip} was not known. However, both crest settlement and bending moment in the piles were measured, so z_{slip} could be determined by trial and error as the back-calculated value giving a good match simultaneously to both the crest settlements and maximum bending moment magnitude in the first earthquake.

Figure 14 shows the effect of pile resistance and geometric re-grading (change in β) on the yield acceleration compared to an unreinforced slope using the first earthquake (EQ1) of test AA01 in each case to determine the effects of the pile reinforcement for an identical input motion. Only the positive (downslope) accelerations have been shown for clarity. It can be seen how the yield acceleration is strongly influenced by the pile resistance for small deformations when the ground motion exceeds the yield acceleration. The pile resistance is mobilised rapidly with slip (consistent with Figure 13). Motion of the slope causes re-grading (geometric hardening) in both the reinforced and unreinforced cases. This is a much more gradual process than the pile resistance mobilisation and the yield acceleration is subsequently seen to increase non-linearly throughout the remainder of the earthquake.

4.4 Results

The input motion used in the sliding block analyses was the acceleration time history measured at accelerometer No. 8 (Figure 10) which represents the accelerometer at the base of the centrifuge model. This is consistent with the approach for unreinforced slopes presented in [1]. Figure 15 shows a comparison of predicted and measured response for S/B = 7.0. The inferred slip plane depth giving this result was z_{slip} = 1.75 m. It should be noted that the slip pane depth for the unreinforced slope is 0.5 m ([1]). Figure 16 shows a similar comparison for S/B = 4.7 (for z_{slip} = 1.77 m) and Figure 17, the comparison for S/B = 3.5 (z_{slip} = 1.65 m).

Considering Figures 15-17 together, it can be seen that in general, the new sliding block method slightly under-predicts deformations in the initial earthquake, though this is worst for the widest spacing and the prediction at closer S/B ratios (a more likely case for design to have the most reinforcing effect) becomes significantly better. Deformations in subsequent earthquakes (e.g. strong aftershocks) are generally slightly over-predicted, which for use in whole-life design of a piled slope (with very many earthquakes), would be conservative. The maximum bending moments reach a limiting value in the first earthquake, in each case representing the peak moment associated with the soil in the slipping mass yielding around the pile. The centrifuge test data suggests proportionally small increases in induced moment in subsequent aftershocks. Increases in subsequent earthquakes are also suggested in the sliding block model due to the reducing value of β_i, but these are much smaller in magnitude. The difference be the result of a small amount of rigid body rotation in addition to the pile bending (rigid body rotation is not incorporated into the current implementation of the sliding block model). The effect of localised non-linearity (through g_m) has a modest effect, resulting in slightly larger deformations for the same amount of induced bending moment in the piles. In each case, the yield acceleration can be seen to exhibit the same characteristics as described in Figure 14, namely an initial rapid mobilisation of the pile resistance, followed by subsequent increases due to geometric hardening. It is noticeable that the maximum bending moments in the centrifuge test data in EQ1 have a stepped appearance, initially mobilising half the ultimate resistance during the large acceleration spikes occurring between 10-15 s, before increasing to the ultimate value based on soil yield around the pile. This would be consistent with the SPI model being stiffer than the actual behaviour (i.e. P is mobilised over a smaller amount of deformation in the model) and so there is potentially still some improvement that could subsequently be made to the SPI model. However, given the simplifications and assumptions in the current implementation, it appears to provide consistent and largely accurate predictions of slope and pile response to large deformations over multiple successive earthquakes.

Figure 18 shows the bending moment distributions as a function of depth at the end of EQ1 for the instrumented pile cases discussed previously. It can be seen that while the magnitude of the peak bending moment and the moment distribution above the inferred slip plane depth appear to be well predicted, the position of the peak moment and the moments below this depth are under-predicted. However, the shape of the predicted and measured curves are similar. These two observations suggest that the critical length of the piles (L_c) is longer than that predicted using Equation (11). The parameter g_m was incorporated to account for reduction in the operative shear modulus in the near-field (due to pile deformation) compared to the free-field values (Figure 11), but this is shown to only have a modest (though positive) effect on the moments. The zero moment point from the centrifuge data and the increased moments at depth would be consistent with a small amount of rigid body rotation, superimposed onto the pile bending mechanism incorporated within the model. Nonetheless, in each case the magnitude of the peak bending moment is well predicted in each case and so the model would appear to be adequate for use in design (determination of pile size and spacing), so long as the pile is designed to have uniform moment capacity with depth, and this is based on the maximum value.

5. *A priori* determination of z_{slip}

In the forgoing validation, the sliding block method was used to obtain (simultaneously) good predictions of slope displacements and pile bending moments, allowing the empirical estimation of z_{slip}. However, for practical use it would be more useful if an *a priori* determination of z_{slip} could be made, for which it would be necessary to find the optimal position of the slip surface in the piled slope. Here, the Discontinuity Layout Optimisation (DLO) technique was used to achieve this [28]. DLO essentially performs upper-bound plasticity analysis in soils with associative flow, via a virtual work (energy balance) type approach. This approach is common for determining collapse loads of geotechnical systems (e.g. bearing capacity of shallow foundations [29]) but requires the critical failure mechanism to be identified (i.e. the configuration of slip lines forming a mechanism which gives the lowest collapse load or least upper-bound). DLO provides an efficient way of identifying this mechanism from all possible combinations of discontinuities that can be formed by linking regularly spaced nodes across a grid, and allows pseudostatic earthquake accelerations to be accounted for [30]. As in [1], LimitState:GEO, v2.0 software was used to calculate the most critical (lowest) upper-bound mechanism by DLO for the geometry and properties of the centrifuge model.

To allow soil yield around the piles in what is otherwise a two-dimensional analysis, the piles were represented as ‘engineered elements’ [31] which allow relative displacement between the soil and each node of this element based on the exceedence of a limiting value of resistance (i.e. the maximum value of P in Figure 13). Three main parameters are required to define the properties of engineered elements: (i) lateral resistance per unit length and width to lateral displacement (N); (ii) axial resistance per unit length and width, (T); and (iii) moment resistance of the element per unit width (pile M_{ult}). A linear variation with depth was assumed for both lateral and axial resistance:

$$T = T_c + T_q . \sigma'_{v0} \tag{25}$$

$$N = N_c + N_q . \sigma'_{v0} \tag{26}$$

The spacing ratio was taken into account in determining the parameters in Equations (25) and (26), so that they represent equivalent values per unit length of the slope. As the pile elements have their tops at the surface of the slope where both resistances are expected to be zero, $T_c = N_c = 0$. The depth-dependent parameters T_q and N_q are given by:

$$T_q = \frac{4.B.(2K_o).\tan\delta'}{S} \tag{27}$$

$$N_q = \frac{{K_p}^2}{(S/B)} \tag{28}$$

where $K_p = (1 + \sin\upsilon')/(1 - \sin\upsilon')$ is the passive earth pressure coefficient and δ' is the interface friction angle between the pile and the soil (based on interface shear test data reported in [10]). T_q therefore represents the axial shaft capacity for a square pile in sand, while N_q is a lateral bearing capacity factor, based on [32]. The moment capacity of the piles, divided by the pile spacing, was used in determining the value of M_{ult}.

While the strength of the soil over a wide strain range was approximated by υ^* in the sliding block analyses, for determining the initial position of the yield surface, the peak friction angle must strictly be used. For stability problems in cohesionless soils it is important to model the true variation of υ'_{pk} with depth (where the strength reduces with increased depth and confining stress due to dilation suppression [33]), to avoid the trivial solution of a failure mechanism forming along the surface of the slope. This was modelled by dividing the soil into multiple 0.5 m thick layers over the top 8 m of soil such that each layer can be assigned an independent angle of friction. Figure 19 shows the variation of υ'_{pk} used in the DLO analyses based on the results of direct shear tests of the sand used in the centrifuge tests, reported in [1].

The value of z_{slip} predicted by DLO was 1.50 m (insensitive to S/B for the parameters used) for the piled slope cases. This is very close to the values of between 1.65 – 1.77 m inferred from the centrifuge test results for the simulations using the Chi-Chi input motion and the value of 1.45 m inferred for test AA16 (Kobe motion) and would suggest that DLO can be used to estimate the required z_{slip} for class A predictions. However, this depends on the sensitivity of the Newmark analysis to this parameter. The centrifuge tests were therefore reanalysed using the sliding block model with the value of z_{slip} predicted from DLO and the results (in terms of prediction of crest settlement and M_{max}) are shown in Figure 20 (filled markers) along with the results using back-calculated z_{slip} values for comparison (hollow markers). Using the DLO value of z_{slip}, there is a general increase in the displacements predicted but a significant reduction in M_{max}. The predictions also become worse with further strong shaking, but are very good in EQ1. Over-prediction of displacements will generally result in a more conservative design for a given tolerable amount of slope deformation. Under-prediction of bending moments suggests that a substantial factor of safety should be applied if the calculated moments are to be used to size/detail the piles. In this case, based on the data in Figure 20, a factor of safety of 2.0 is indicated.

6. Conclusions

The modified Newmark procedure developed by Al-defae et al., [1] for predicting slip in unreinforced cohesionless slopes including strain-induced geometric hardening (slope re-grading) has here been modified to be applicable to pile–reinforced slopes (incorporating strain-dependent pile resistance) to allow estimation of permanent seismic deformation in piled slopes. This is achieved through modifying the yield acceleration at each time step by incorporating mobilised pile resistance forces consistent with the current amount of relative soil-pile movement. This simplified combined model needs only relatively basic information about the soil (υ', γ, v, G_0, u, c'), slope geometry (β, H, L), pile properties/layout (B, EI, S, plus M_{ult} for checking capacity is not exceeded) and earthquake (a time history and dynamic amplification factor for estimating a_{max}), and an estimated slip plane depth (z_{slip}). A procedure for estimating z_{slip} via an optimised upper-bound plasticity analysis (here conducted using Discontinuity Layout Optimisation, DLO) was also proposed.

The model was validated against a database of centrifuge test results having different pile-to-pile spacing and earthquake excitations in cohesionless soil. The permanent slope deformations and maximum induced bending moments (M_{max}) were predicted extremely closely for first earthquake conditions using back-calculated values of z_{slip}. Using the DLO procedure to estimate this parameter resulted in similarly good deformation estimates, but under-prediction of M_{max} due to the high sensitivity of M_{max} to z_{slip}. This implies that there is scope to develop the z_{slip} predictions further. The method can also be applied to subsequent strong shaking (aftershocks), but the predictions, while reasonable, become poorer as greater numbers of subsequent earthquakes are applied (generally over-estimating crest deformation and under-estimating M_{max}).

The model will be useful in seismic design for determining appropriate pile layouts and sizing/detailing to meet a prescribed amount of slope deformation at the crest while ensuring that the piles remain elastic. This will provide a useful screening tool for identifying promising configurations for further, more detailed numerical (Finite Element) modelling which can fully verify dynamic behaviour.

Acknowledgements

The authors would like to express their sincere gratitude to Mark Truswell and Colin Stark at the University of Dundee for their assistance in performing the centrifuge tests. The first author would also like to acknowledge the financial support of his PhD studies from the Ministry of Higher Education and Scientific Research (MOHESR) of the Republic of Iraq.

References

[1] Al-Defae, A.H., Caucis, K. and Knappett, J.A. Aftershocks and the whole-life seismic performance of granular slopes. *Géotechnique 2013*. **63**(14):1230-1244.

[2] Liang, R.Y. Drilled shaft foundations of noise battier walls and slope stabilisation. Ohio Department of Transportation and the U.S. Department of Transportation 2002, Federal Highway Administration and The University of Akron, Akron, Ohio, 2002, Report no. 44325-3905.

[3] Wang, W. L., Yen, B. C. Soil arching in slopes. *Journal of Geotechnical and Geoenvironmental Engineering 1974:* **105** (GT4): pp. 493-496.

[4] Ito, A.T. & Matsui, T. Method of estimate lateral forces acting on stabilising piles. Japanese Society of Soil Mechanics and Foundation Engineering 1975: **15**(4): 43-59.

[5] Ito, T., Matsui, T. and Hong, W.P. Extended design method for multi-row stabilising piles against landslides. Journal of Soil and Foundation 1982: **22**(1): 1-13.

[6] Hassiotis, S., Chameau, J.L. & Guanaratne, M. Design method for stabilisation of slope with piles. Journal of Geotechnical and Geoenviornmental Engineering, ASCE 1997: **123**(4): 314-323.

[7] Kourkoulis, R., Gelagoti, E., Anastasopoulos, I. and Gazetas, G. Stabilisation of seismically unstable slopes using piles: Parametric Analysis. 5th International Conference on Earthquake Geotechnical Engineering, Santiago, Chile, 2011, Vol.1.

[8] Newmark, N.M. Effect of earthquakes on dams and embankments. Géotechnique 1965: **15**(2): 139-159.

[9] Matasovic, N., Kavazanjian, E. and YAN, L. Newmark deformation analysis with degrading yield acceleration. *Proceeding of Geosynthetics. Vol. 2, Long Beach, California,* USA, March 1997, pp 989-1000.

[10] Al-Defae, A.H. and Knappett, J.A. Centrifuge modelling of the seismic performance of pile-reinforced slopes. *Journal of Geotechnical and Geoenviornmental engineering, ASCE 2014,* (In press).

[11] Michalowski, R.L., and Shi, L. Bearing capacity of footings over two-layer foundation soils. Journal of Geotechnical Engineering 1995: **121**(5): 421–428.

[12] Drescher, A. and Detournay, E. Limit load in translational failure mechanisms for associative and non-associative materials. Géotechnique 1993: **43**(3): 443–456.

[13] O'Neill, M.W., and Murchison J.M. An evaluation of p-y relationships in sand. A Report to the American Petroleum Institute, PRAC 82-41-1, the University of Houston-University Park, Houston, Texas, 1993.

[14] American Petroleum Institute, API. Recommended practice for planning, designing, and constructing fixed offshore platforms. API Recommended Practice 2A 2000 (RP-2A-WSD), 21 Edition.

[15] Randolph, M.F. The response of flexible piles to lateral loading. Géotechnique 1981: **31**(2): 247-259.

[16] Hardin, B.O. and Drnevich, V.P. Shear modulus and damping in soils: Design Equation and Curves. Journal of Soil Mechanics and Foundation Engineering Division 1972: **98**(SM7):667-692.

[17] Seed, H.B., and Idriss, I.M. Simplified procedure for evaluating soil liquefaction potential. Journal of Soil Mechanic and Foundation Division 1971: **97** (9): 1249–1273.

[18] Idriss, I.M. An update to the Seed-Idriss simplified procedure for evaluating liquefaction potential. In Proceedings, TRB Workshop on New Approaches to Liquefaction, FHWA-RD-99- 165, FHWA, Washington, D.C, 1999.

[19] Pradel D. Procedure to evaluate earthquake-induced settlements in dry sandy soils. Journal of Geotechnical & Geoenvironmental Engineering 1998: **124** (4): 364-368.

[20] Hayward, T., Lees, A., Powrie, W. & Smethurst. Centrifuge modelling of a cutting slope stabilised by discrete piles. TRL471 report 2000, Transport Research Laboratory, Berkshire, UK.

[21] Poulos, H.G. and Davis, E.H. (1980). Pile foundation analysis and Design. John Wiley & Sons Inc., New York.

[22] Alizadeh, M. and Davisson, M.T. (1970). Lateral load tests on piles – Arkansas River Project. Journal of the Soil Mechanics & Foundations Division, ASCE, 96(SM5): 1583-1604.

[23] Fleming, W.G. K., Weltman, A.J., Randolph, M.F. and Elson, W.K.,. Piling engineering. 3rd Edition. Halsted Press, New York, NY100116, USA, 2009.

[24] Bertalot, D. Behaviour of shallow foundations on layered soil deposits containing loose saturated sands during earthquakes. PhD Thesis, University of Dundee, UK, 2013.

[25] Brennan, A.J., Thusyanthan, N.I. and Madabhushi, S.P.G. Evaluation of shear modulus and damping in dynamic centrifuge tests. Journal of Geotechnical and Geoenviornmetnal Engineering 2005: **131**(12): 1488-1497.

[26] Pan, J., Goh, A., Wong, K. and Teh, C. Ultimate soil pressure for piles subjected to lateral soil movement. Journal of Geotechnical and Geoenvironmental Engineering Division 2002: **128**(6): 530-535.

[27] Bransby, M.F. & Springman, S. Selection of load-transfer functions for passive lateral loading of pile groups. Journal of Computers and Geotechnics 1999: **24**(3): 155-184.

[28] Smith, C.C. and Gilbert, M. Application of discontinuity layout optimization to plane plasticity problems. Proc. Royal Soc 2007 A: Mathematical, Physical and Engineering Sciences, 463 (2086), October: 2461-2484.

[29] Knappett, J.A. and Craig, R.F. Craig's Soil Mechanics (8th Edition), Spon Press, Abingdon, UK, 2012.

[30] Smith, C.C. and Cubrinovski, M. Pseudo-static limit analysis by discontinuity layout optimization: Application to seismic analysis of retaining walls. Soil Dynamics and Earthquake Engineering 2011: **31**(10): 1311-1323.

[31] Clarke, S.D., Gilbert, M. and Smith, C.C. Modelling discrete soil reinforcement in numerical limit analysis. Canadian Geotechnical Journal: **50**(7): 705-715.

[32] Fleming, W.G.K., Weltman, A.J., Randolph, M.F. and Elson, K. Piling Engineering (3rd Edition), Taylor and Francis, Abingdon, UK, 2009.

[33] Bolton, M.D. The strength and dilatancy of sands. Geotechnique 1986: **36**(1):65-78.

Notation

Roman:

A	Monotonic/cyclic loading factor for P-y curve
a	Shear strain constant
a_{max}	Peak acceleration at ground surface
B	Pile width
b	Shear strain constant
c'	Cohesion intercept
$C_{1,2}$	Lateral pile resistance constants
d	Incremental slope-parallel slip
D_{eq}	Equivalent diameter of a circular pile
D_r	Relative density
e	Natural void ratio
E_p	Pile Young's Modulus for equivalent solid circular section
EI	Bending stiffness (pile)
G	Shear modulus
G_o	Small strain modulus
G_c	Shear modulus associated with critical length
$\bar{G}_{Lc}$	Median value of operative shear modulus over the critical length
g	Acceleration due to gravity (= 9.81 m/s^2)
g_m	Stiffness reduction factor for local non-linearity in stable soil
H	Slope height above toe
k	Subgrade reaction modulus
k_h	Pseudo-static seismic horizontal acceleration (g)
k_{hy}	Yield acceleration (g)
K_0	Lateral earth pressure coefficient (at rest)
K_p	Passive lateral earth pressure coefficient

L Length along slip plane

L_c Critical length of pile (below slip plane)

M Bending moment

M_{max} Maximum induced pile bending moment

M_{ult} Pile bending moment capacity

M_w Moment magnitude

$N_{c,q}$ Pile lateral resistance per unit shaft area (constant, depth dependent)

p_a Atmospheric pressure (= 100 kPa)

p_m P-multiplier (pile shadowing effect)

p_u Ultimate lateral soil-pile resistance (per metre length of pile)

p'_0 Initial mean confining stress

P Pile-soil resistance force (single pile)

r_d Stress reduction factor

S Pile centre-to-centre spacing

$T_{c,q}$ Pile axial resistance per unit shaft area (constant, depth dependent)

u Pore water pressure

y_p Pile lateral deformation (at $0.67z_{slip}$ below soil surface)

y_s Cumulative soil slip

z Depth below ground surface

z_{slip} Depth of slip plane

Greek:

$\alpha_{1,2}$ Stress reduction coefficients

β Slope angle

β_0 Initial slope angle (pre-earthquake)

γ Soil unit weight

γ' Effective (buoyant) unit weight

γ_w Unit weight of water (= 9.81 kN/m^3)

δ'	Interface friction angle
ε_s	Shear strain
$\varepsilon_{s,cyc}$	Cyclic shear strain
φ'	Effective angle of friction
φ^*	Angle of friction (accounting for non-associativity)
φ'_{cs}	Critical state angle of friction
φ'_{pk}	(Secant) Peak angle of friction
v	Poisson ratio (soil)
ρ_c	Homogeneity factor (shear modulus variation with depth)
σ_{v0}	Total overburden (vertical) stress
σ'_{v0}	Effective overburden (vertical) stress
σ'	Normal effective stress
$\tau_{applied}$	Applied shear stress
τ_{av}	RMS average cyclic shear stress
τ_{ult}	Soil shear strength
ψ'	Effective angle of dilation

Table

Table 1: Summary of centrifuge test database for model validation

Test ID	D_r (%)	*S/B*	Input motion	No. of earthquakes
AA01	56	Unreinforced	Chi-Chi	4
AA13	60	7.0	Chi-Chi	4
AA14	57	4.7	Chi-Chi	4
AA15	59	3.5	Chi-Chi	4
AA17	59	Unreinforced	Kobe	4
AA16	57	4.7	Kobe	4

Figures Captions

Figure 1: Slip mechanism in pile-reinforced slope; (a) overall configuration; (b) forces acting on a pile-stabilised slipping soil element.

Figure 2: Simplified model for geometric hardening (slope re-grading) for a slope suffering translational slip (after [1]).

Figure 3: Modelling approach for soil-pile interaction (SPI).

Figure 4: P-y coefficients as a function of friction angle (after [14]).

Figure 5: Stable soil interaction and definition of shear modulus within stable soil.

Figure 6: Relationship between p-multiplier and normalised pile spacing (pile shadowing effect).

Figure 7: Relationship between g_m and pile deformation y_{pi} (effect of non-linearity in stable soil)

Figure 8: Flow chart summarising analysis procedure.

Figure 9: Normalised bending moment curves for piles resisting an infinite slip.

Figure 10: Centrifuge model layout, with instrumented elastic piles shown, dimensions in m prototype scale (mm model scale in brackets).

Figure 11: Comparison of predicted operative shear modulus with depth and centrifuge test observations.

Figure 12: Shear stress, shear strain and shear modulus in test AA14, EQ1: (a) at 2.75 m depth, (b) at 4.50 m depth, (c) at 6.25 m depth.

Figure 13: Calculated SPI curves for centrifuge test conditions.

Figure 14: Effect of pile resistance mobilisation and geometric hardening on slope behaviour; (a) crest settlement; (b) development of yield acceleration.

Figure 15: Validation for test AA13 (S/B = 7.0): (a) Predicted and measured crest settlement; (b) Predicted and measured maximum moment (M_{max}); (c) variation of yield acceleration and input motion.

Figure 16: Validation for test AA14 (S/B = 4.7): (a) Predicted and measured crest settlement; (b) Predicted and measured maximum moment (M_{max}); (c) variation of yield acceleration and input motion.

Figure 17: Validation for test AA15 (S/B = 3.5): (a) Predicted and measured crest settlement; (b) Predicted and measured maximum moment (M_{max}); (c) variation of yield acceleration and input motion.

Figure 18: Predicted and measured bending moments along piles, end of EQ1: (a) Test AA13; (b) Test AA14; (c) Test AA15.

Figure 19: Peak friction angle used to determine initial position of slip surface.

Figure 20: Effect of using DLO-predicted slip plane depth on prediction of slope deformation and maximum pile bending moments.

Figure 1

Click here to download high resolution image

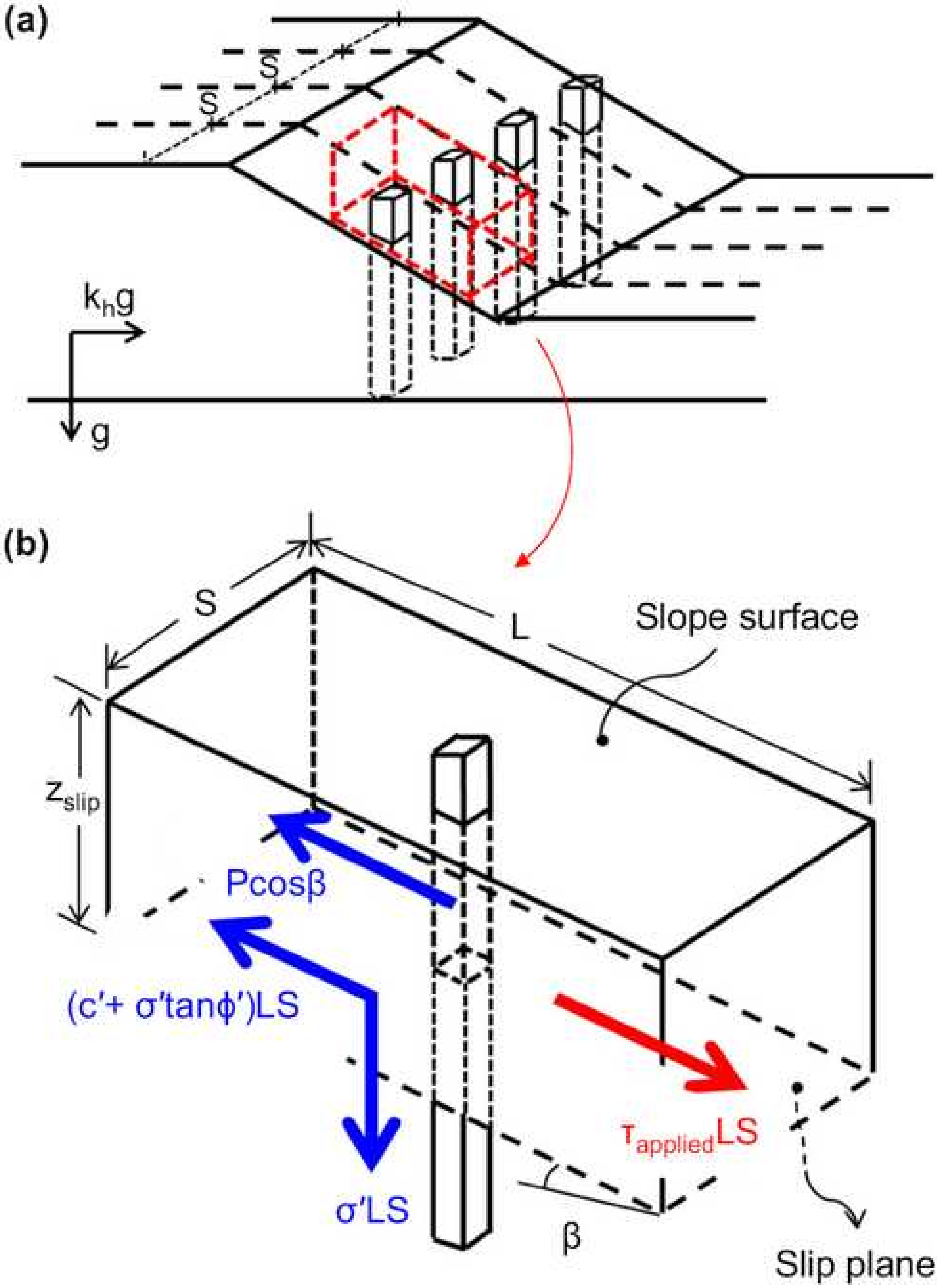

Figure 2
Click here to download high resolution image

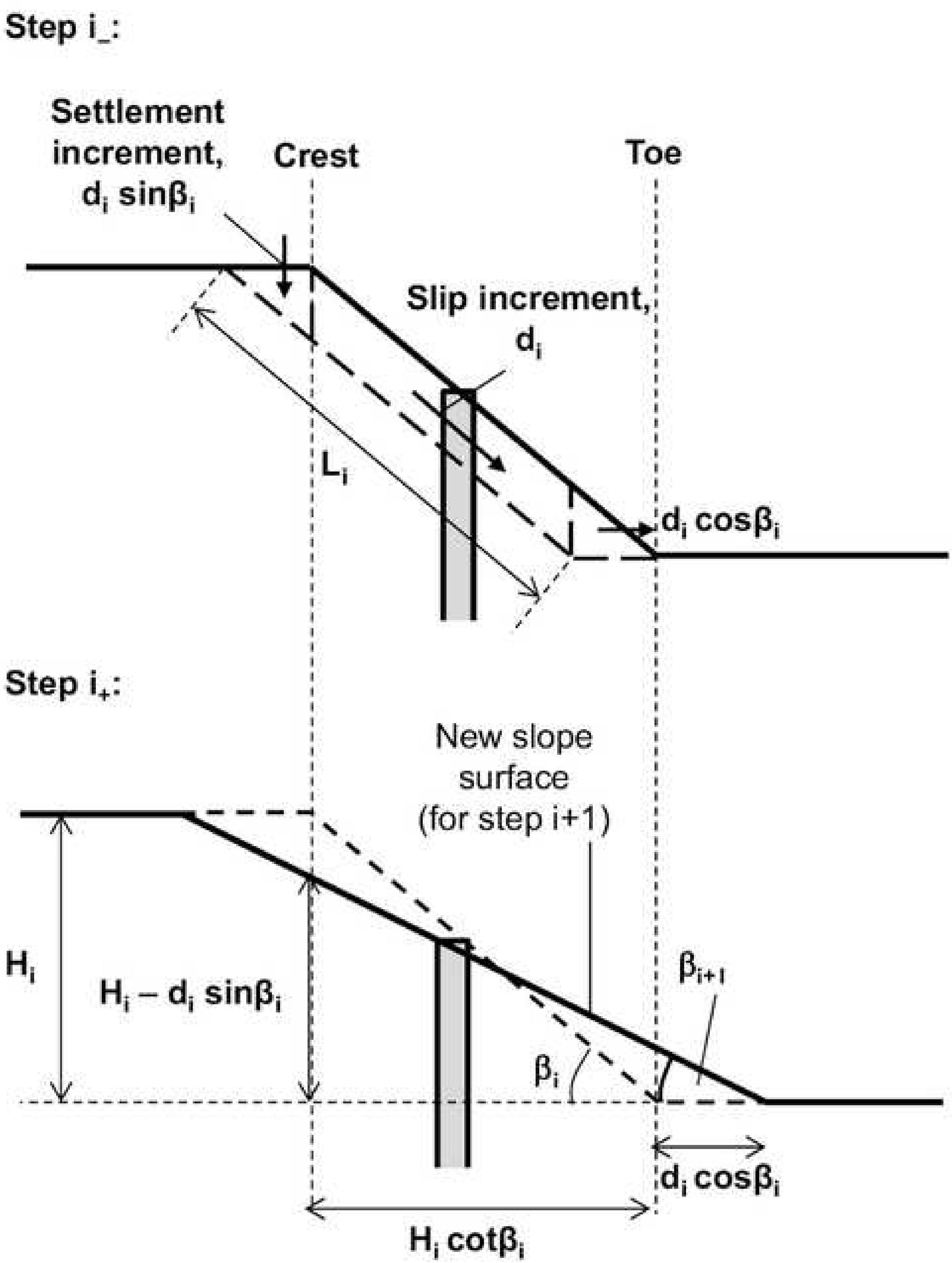

Figure 3
Click here to download high resolution image

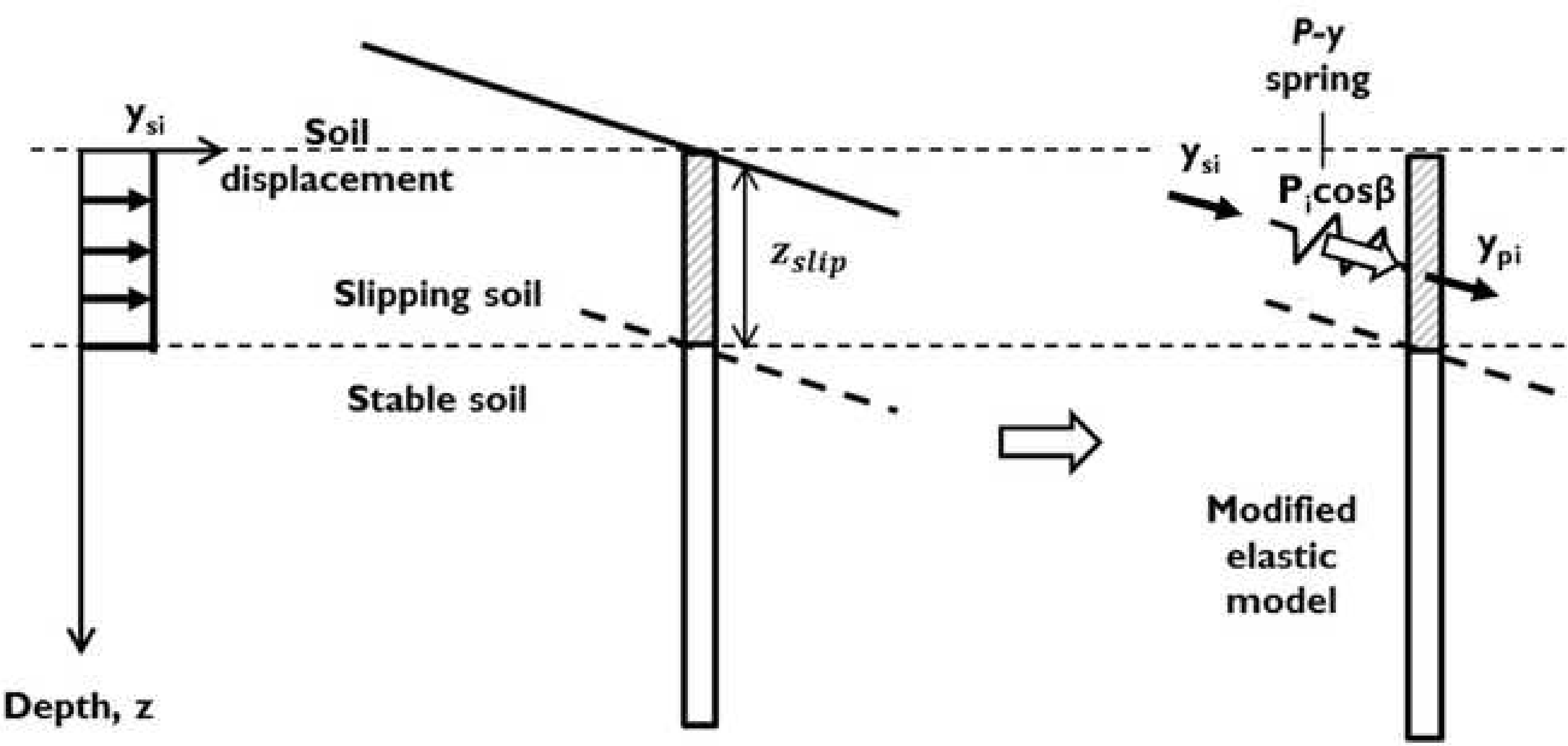

Figure 4
Click here to download high resolution image

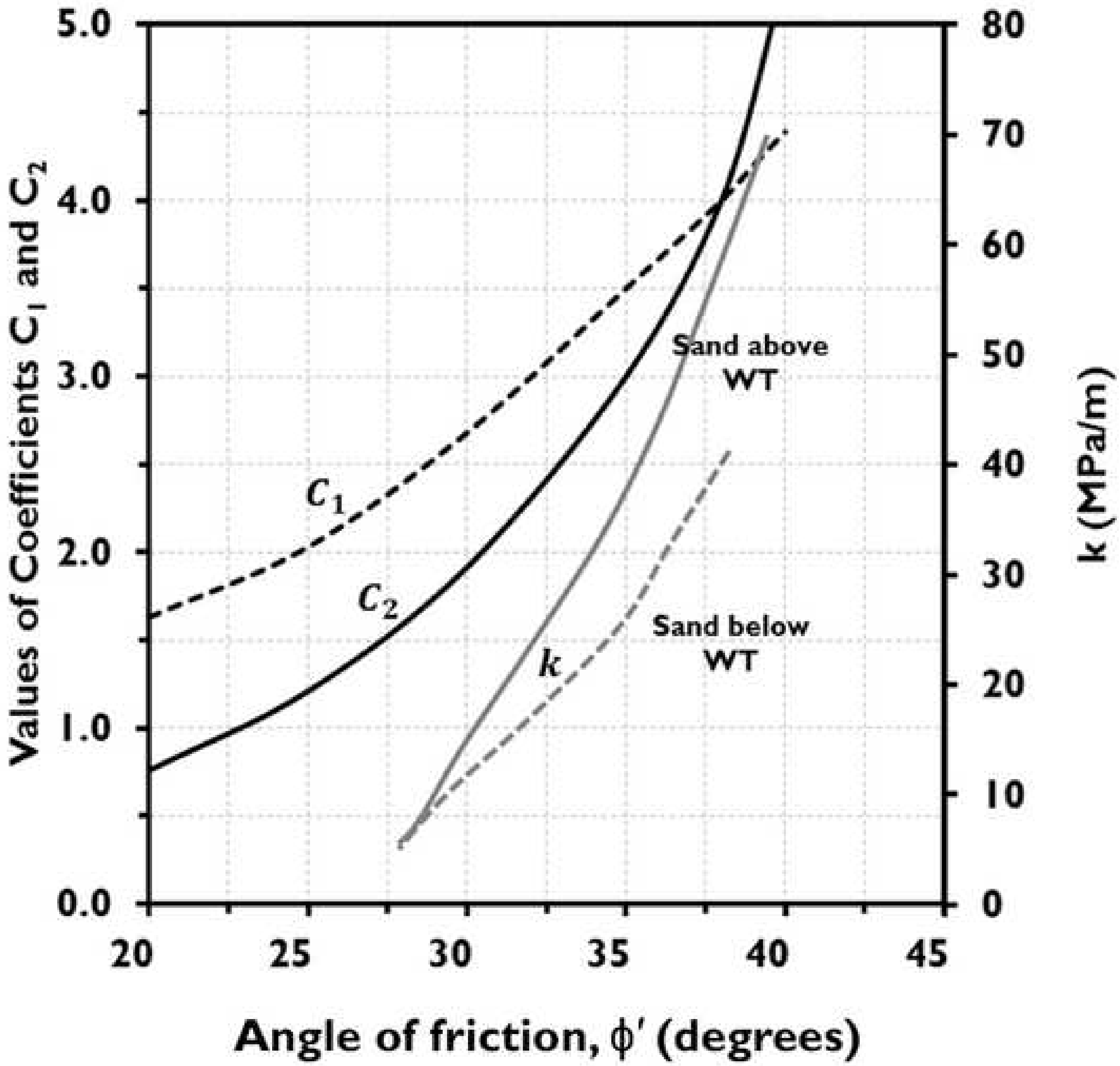

Figure 5
Click here to download high resolution image

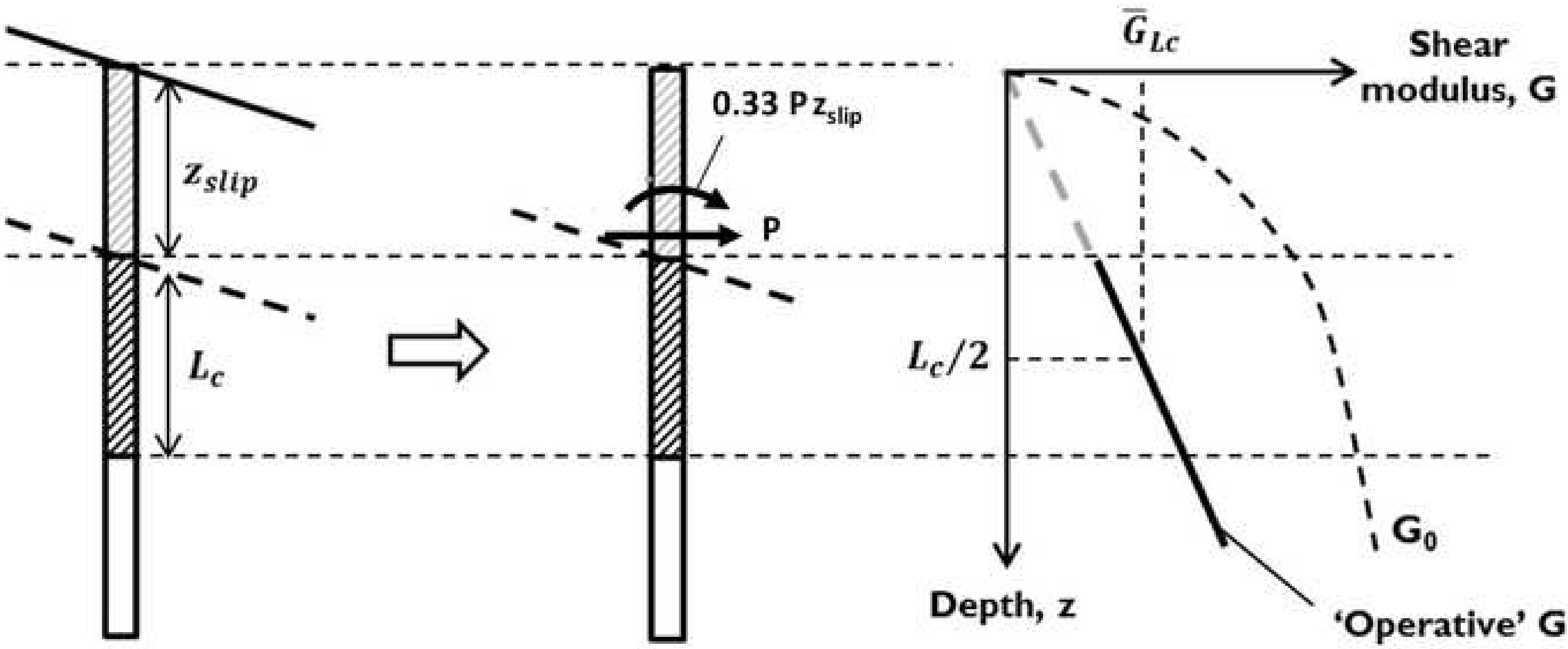

Figure 6
Click here to download high resolution image

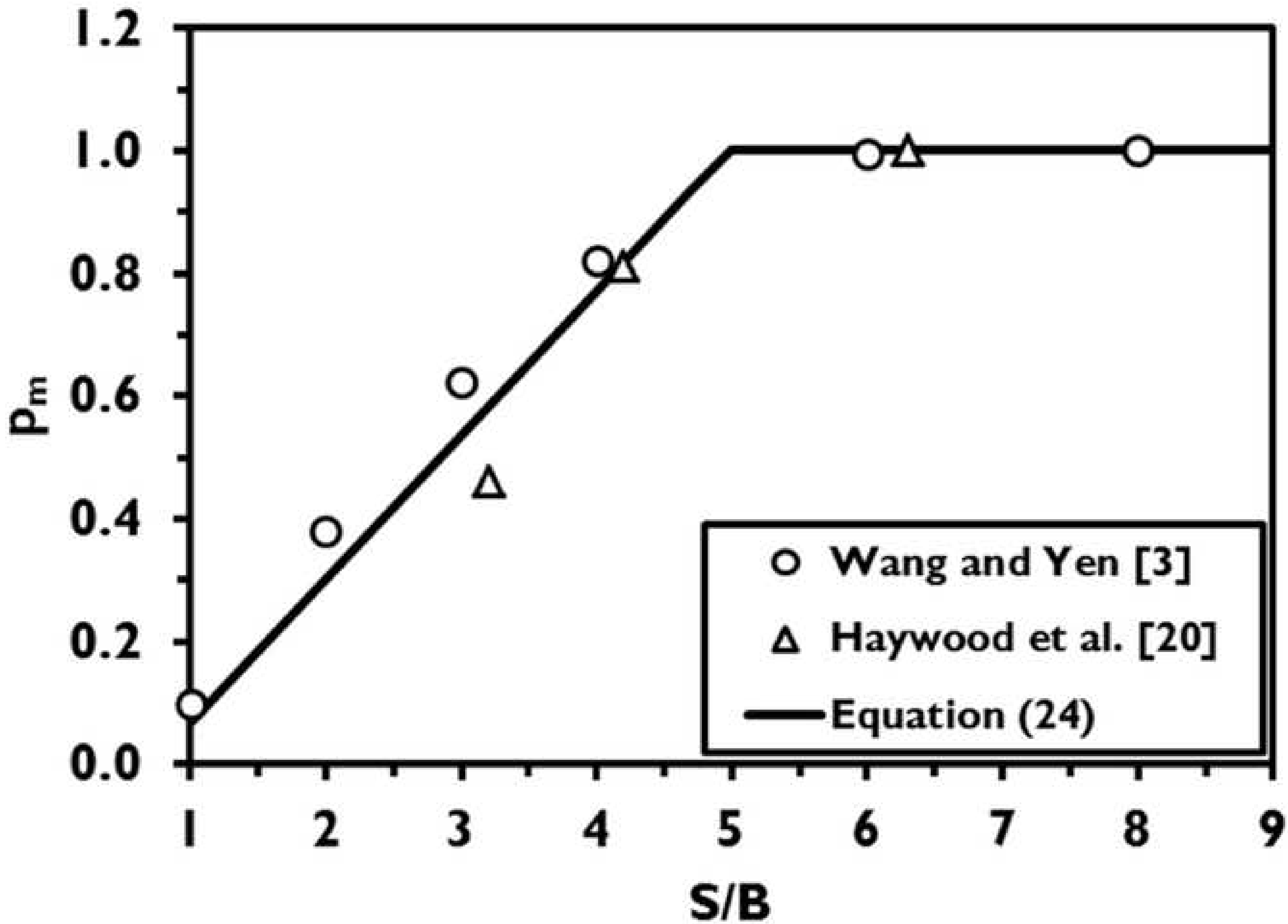

Figure 7
Click here to download high resolution image

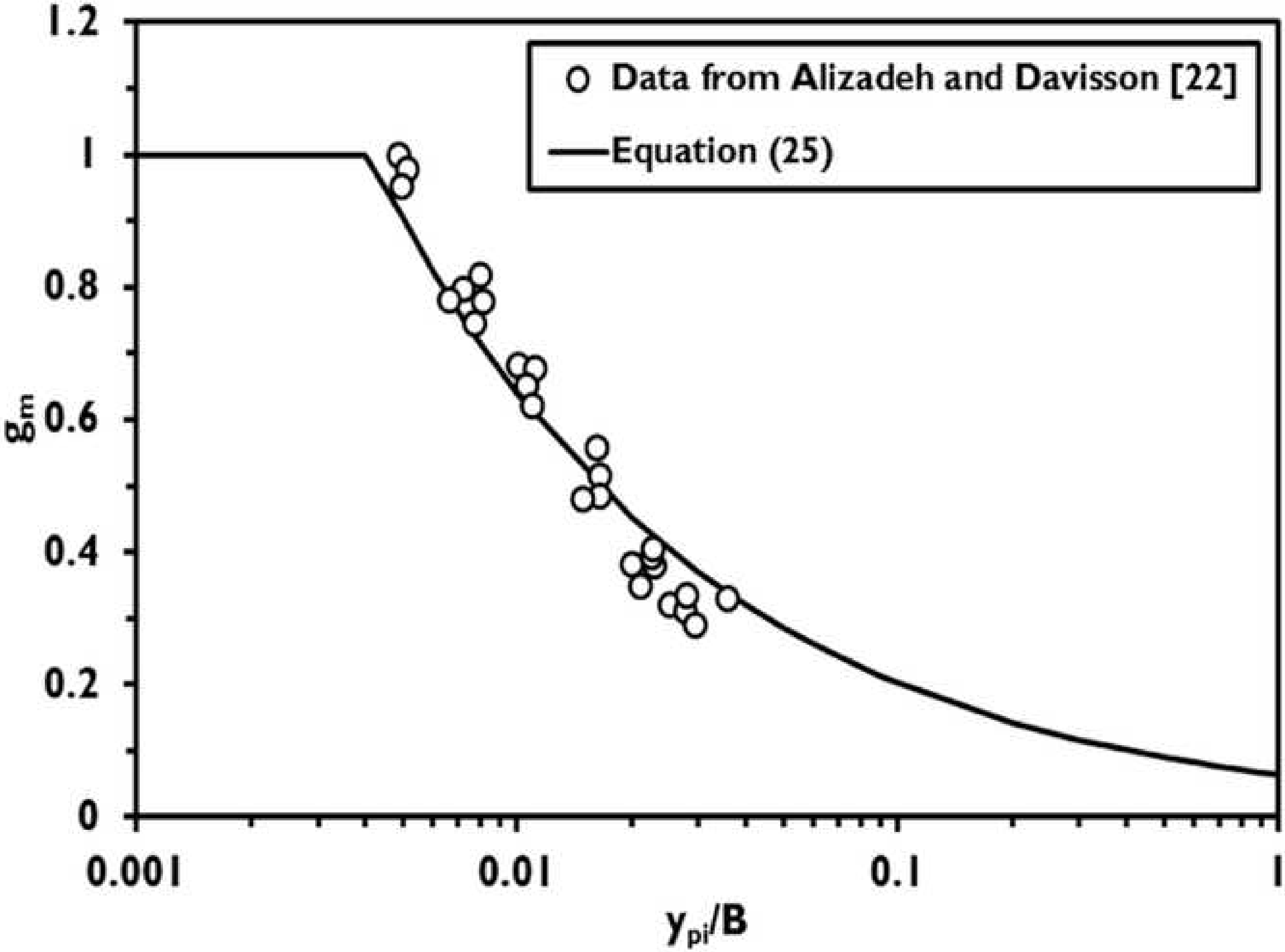

Figure 8
Click here to download high resolution image

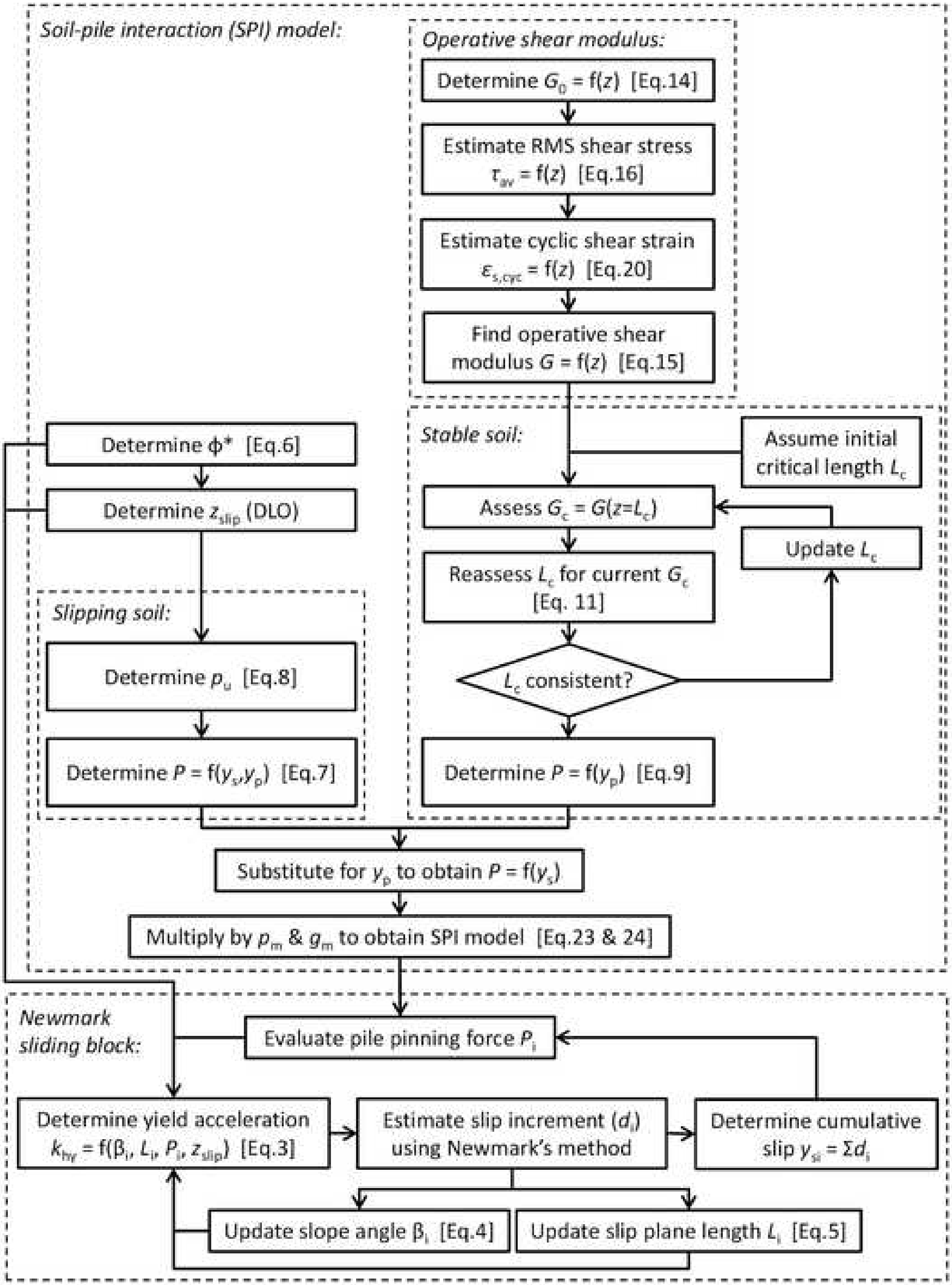

Figure 9
Click here to download high resolution image

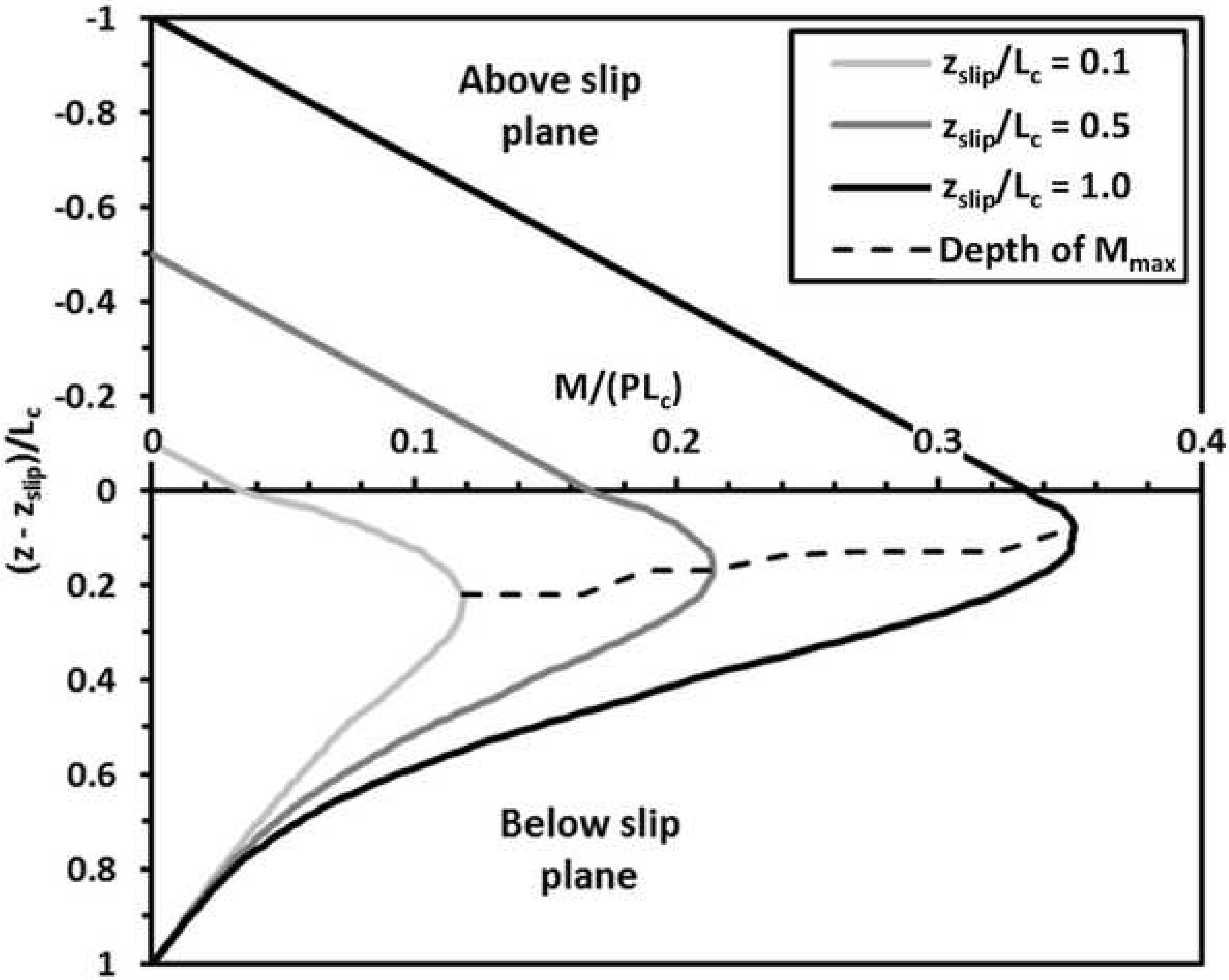

Figure 10
Click here to download high resolution image

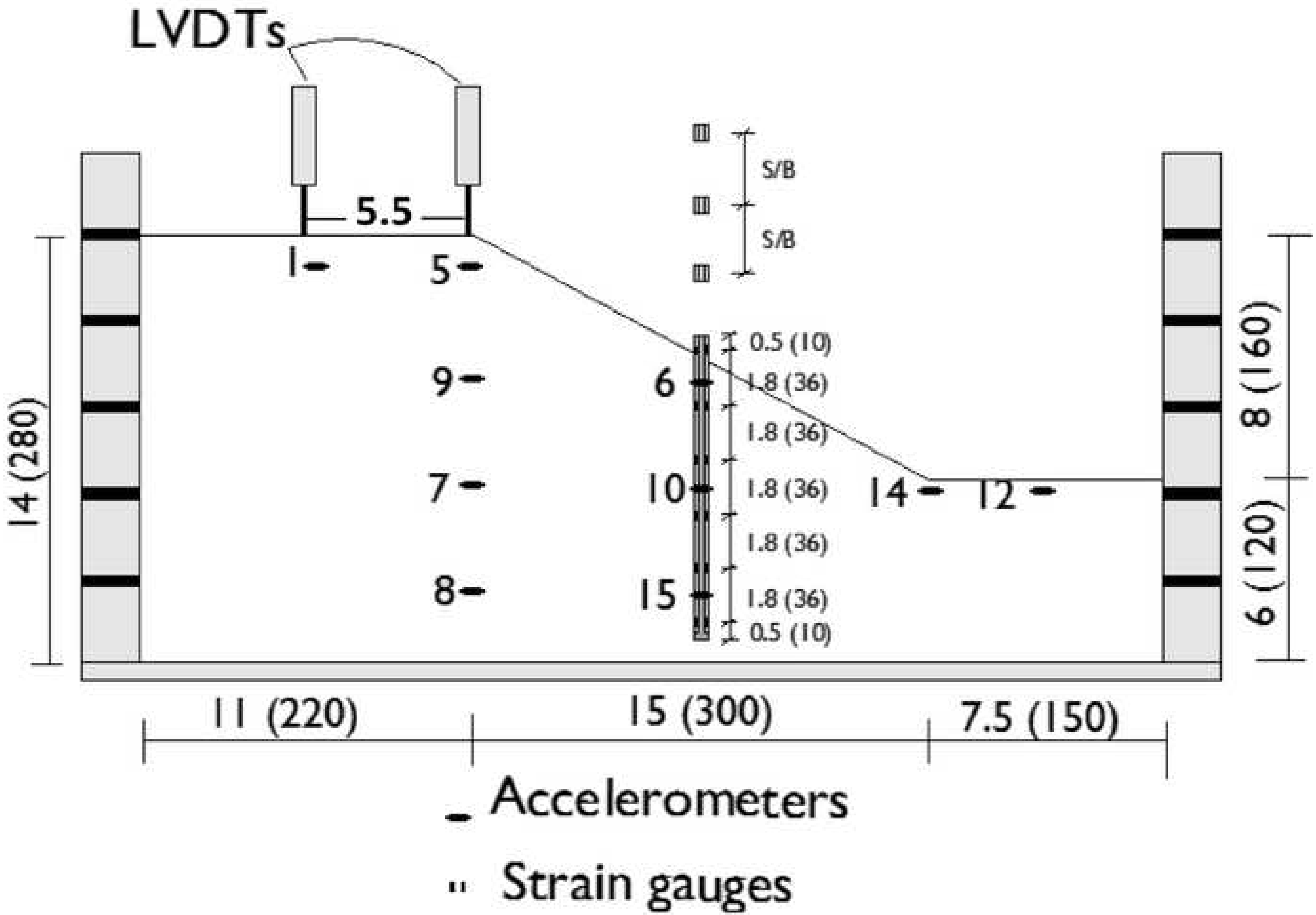

Figure 11
Click here to download high resolution image

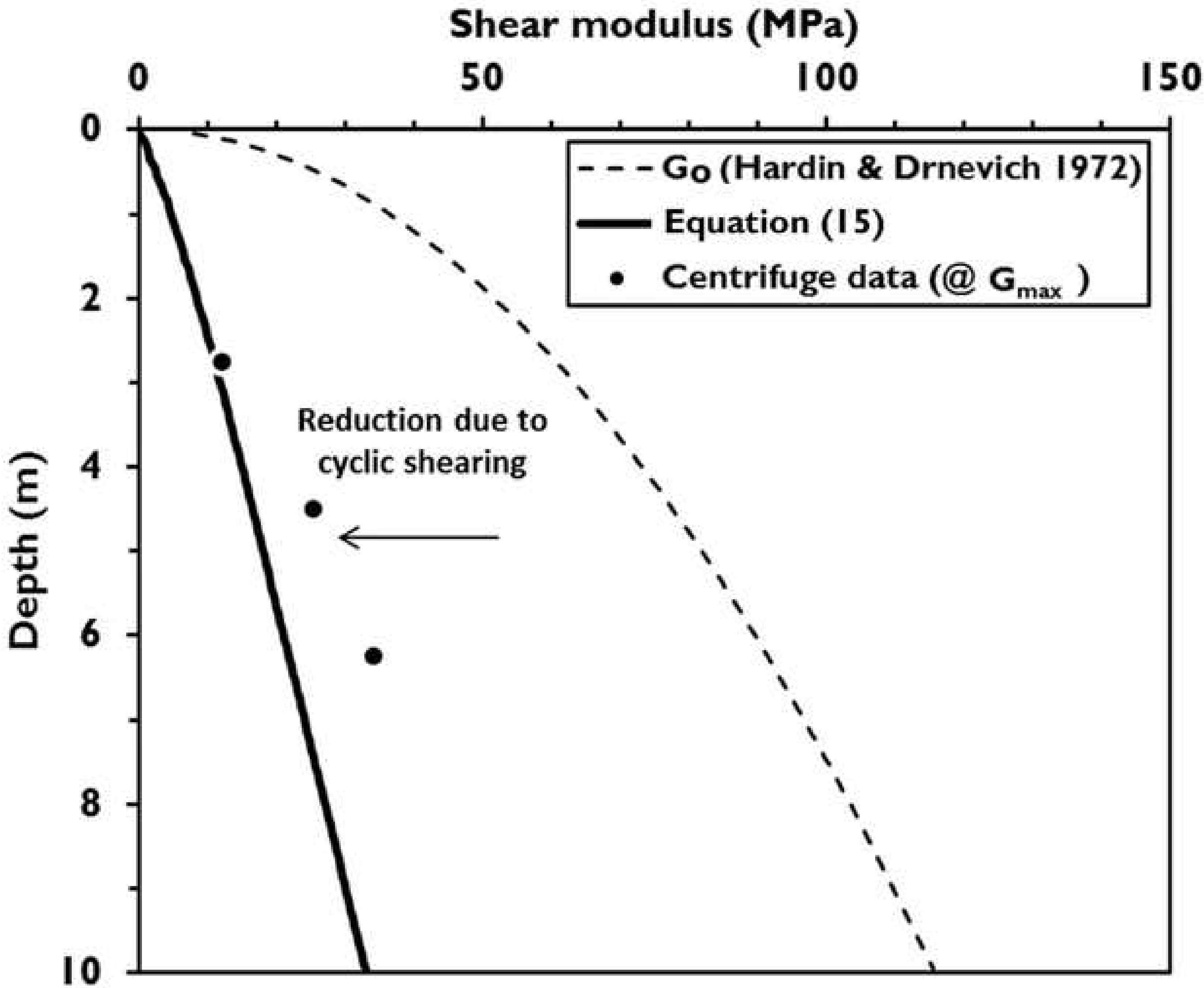

Figure 12
Click here to download high resolution image

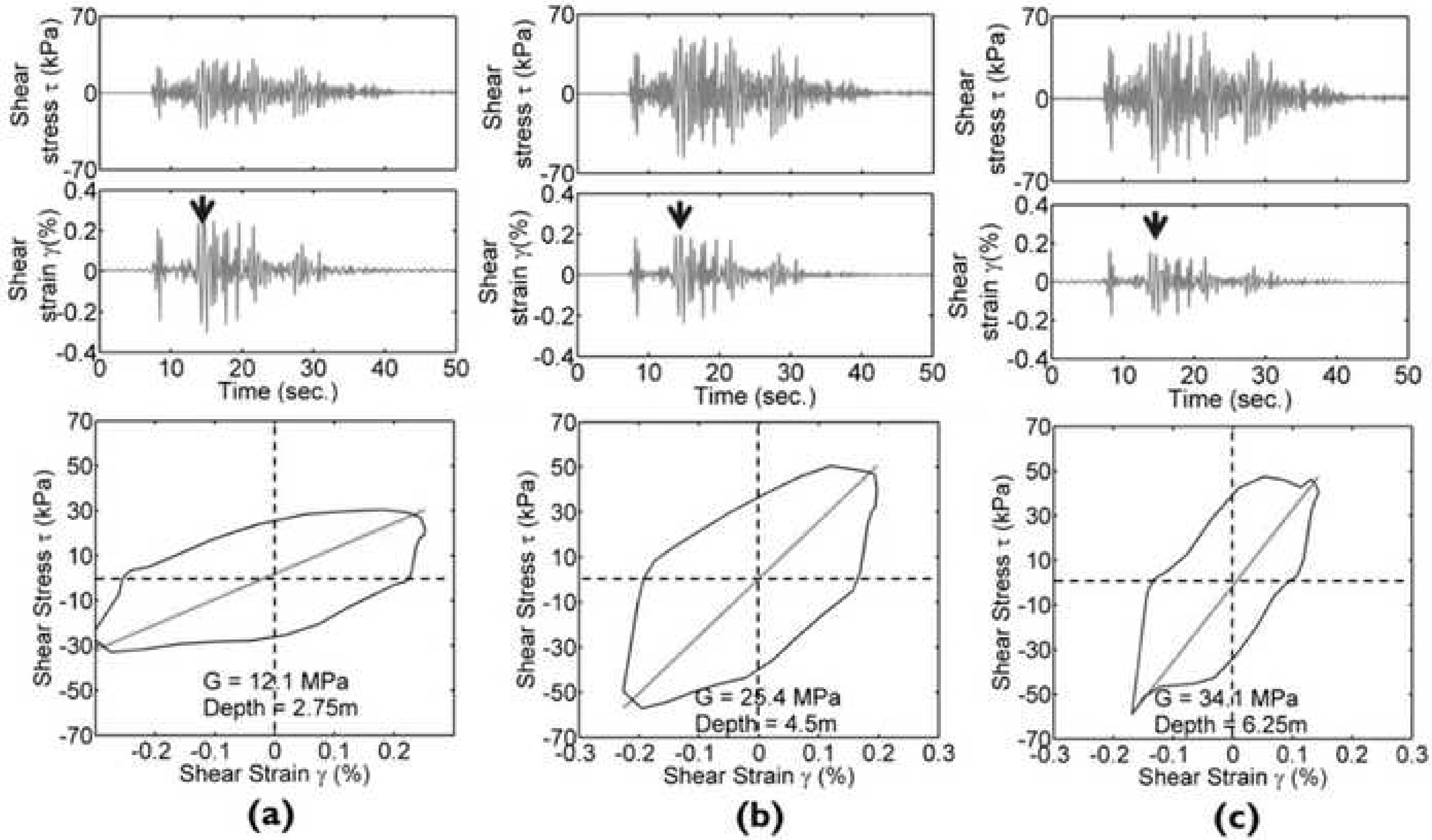

Figure 13
Click here to download high resolution image

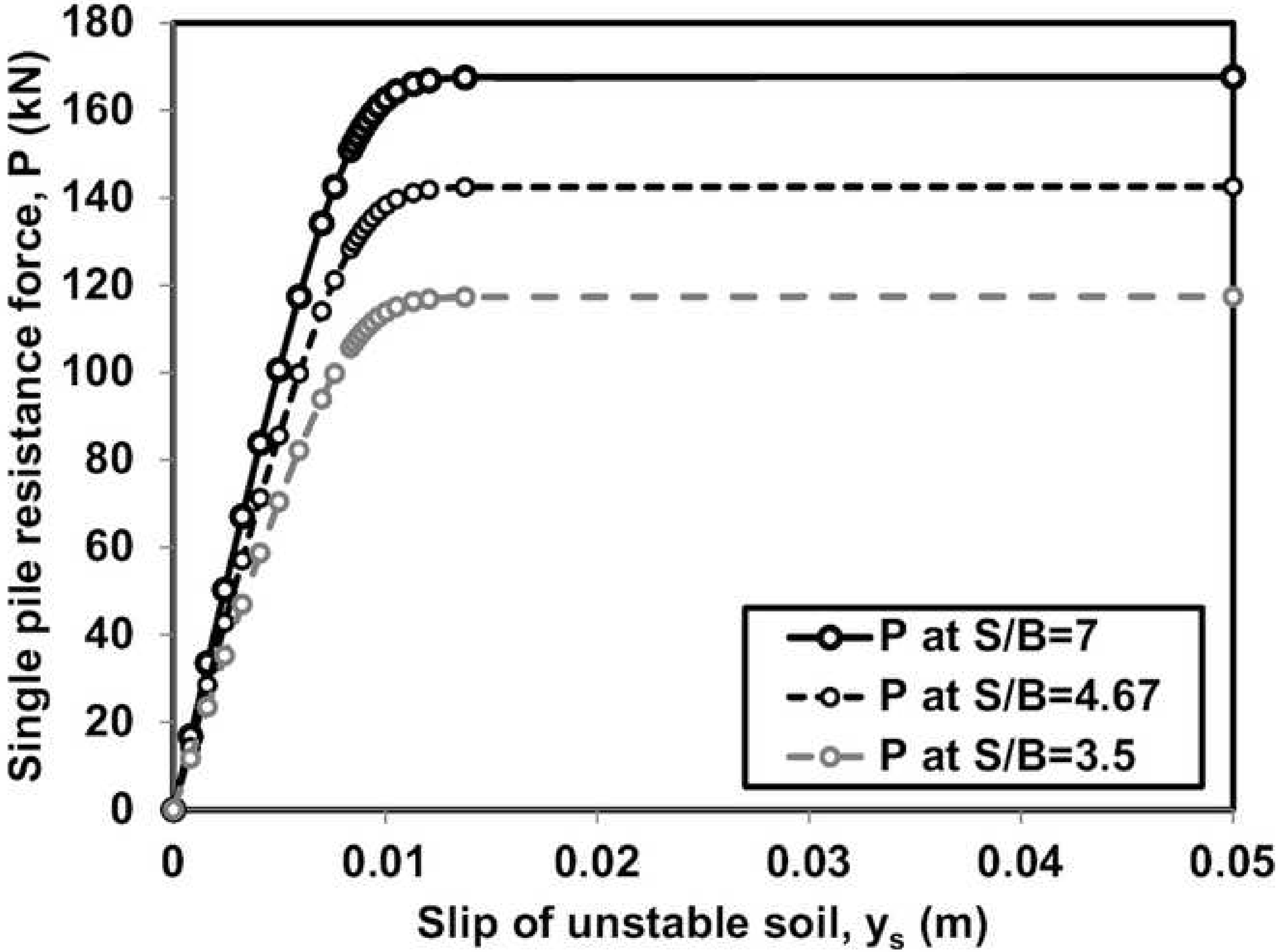

Figure 14
Click here to download high resolution image

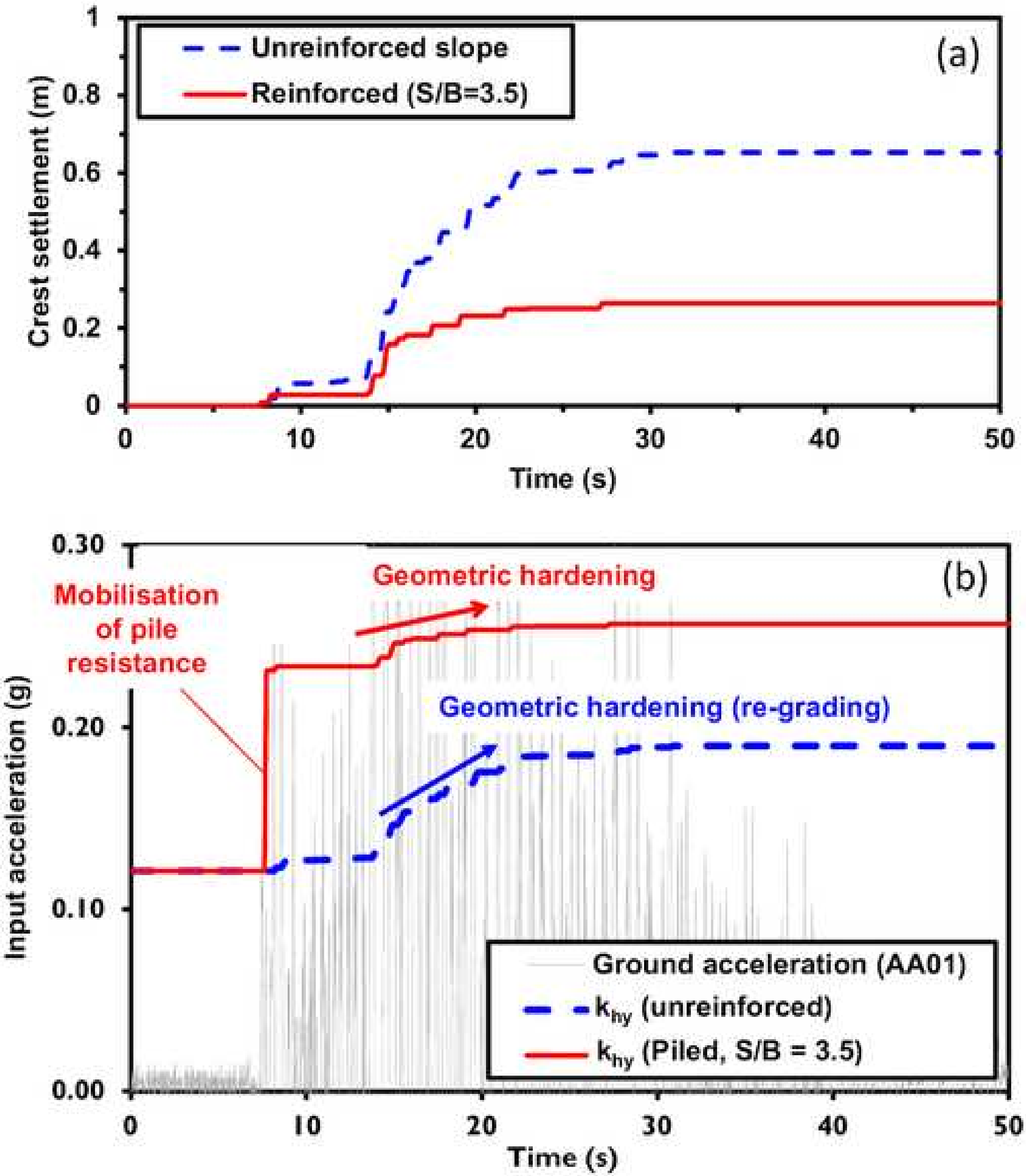

Figure 15
Click here to download high resolution image

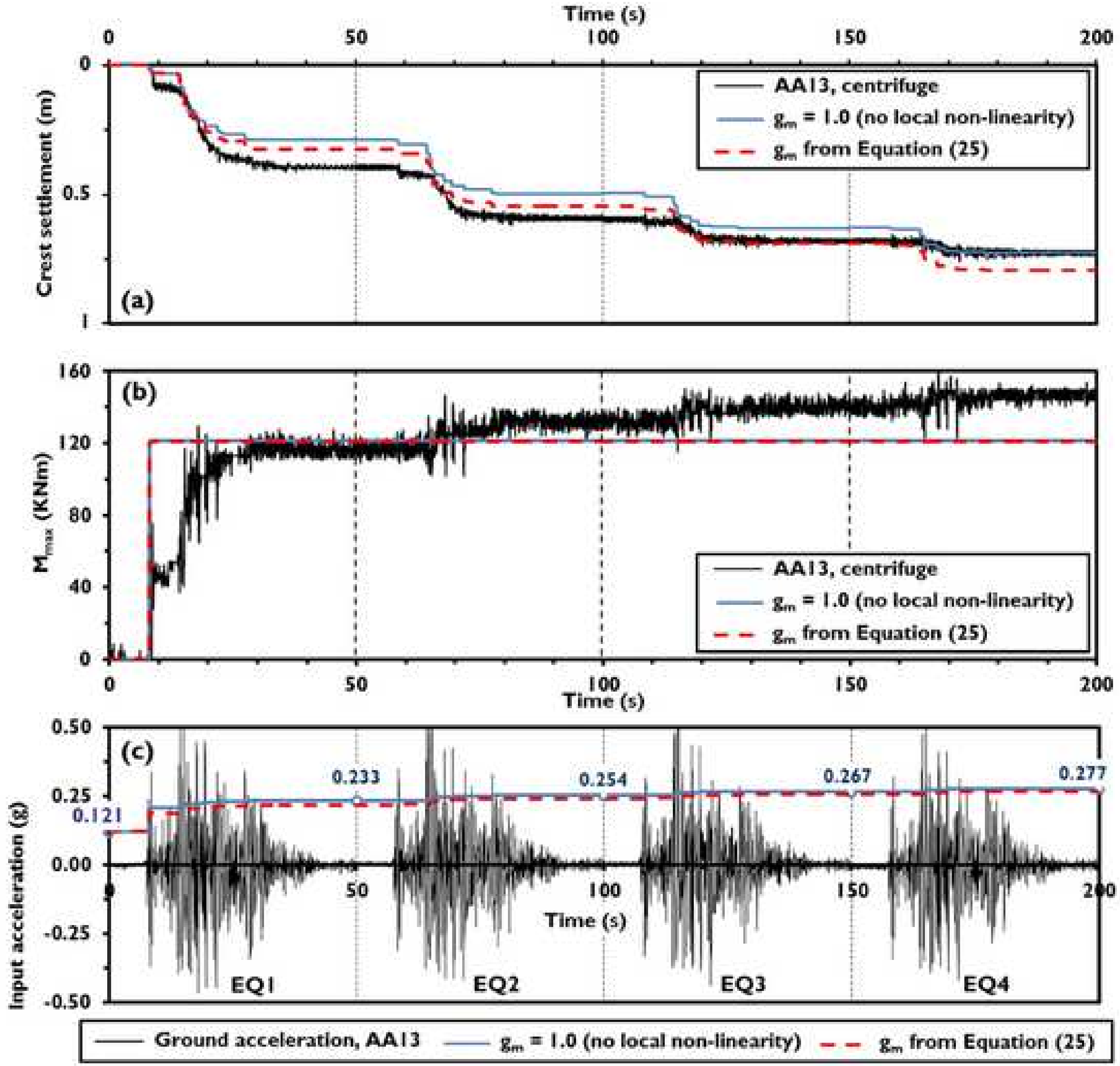

Figure 16
Click here to download high resolution image

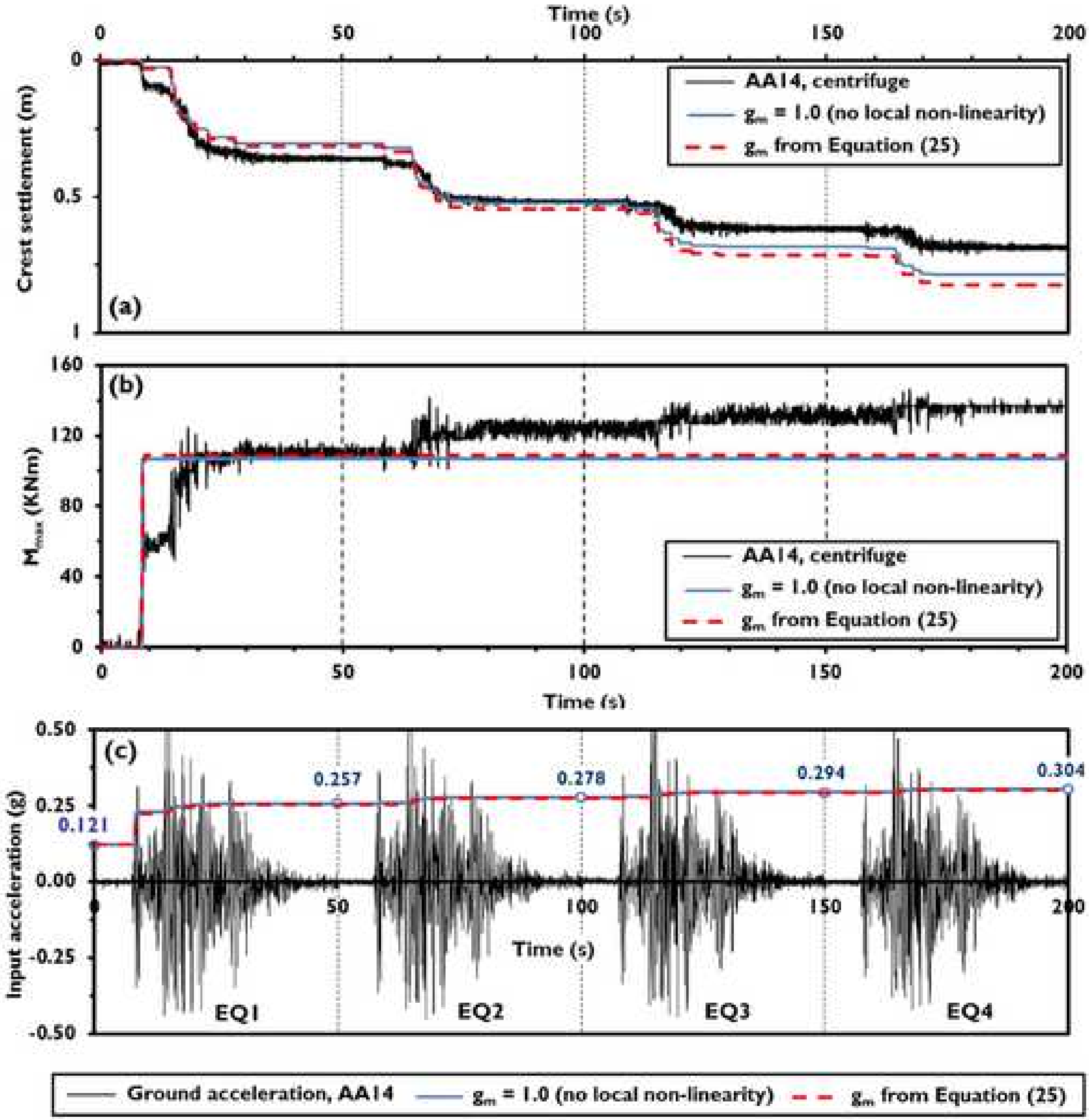

Figure 17
Click here to download high resolution image

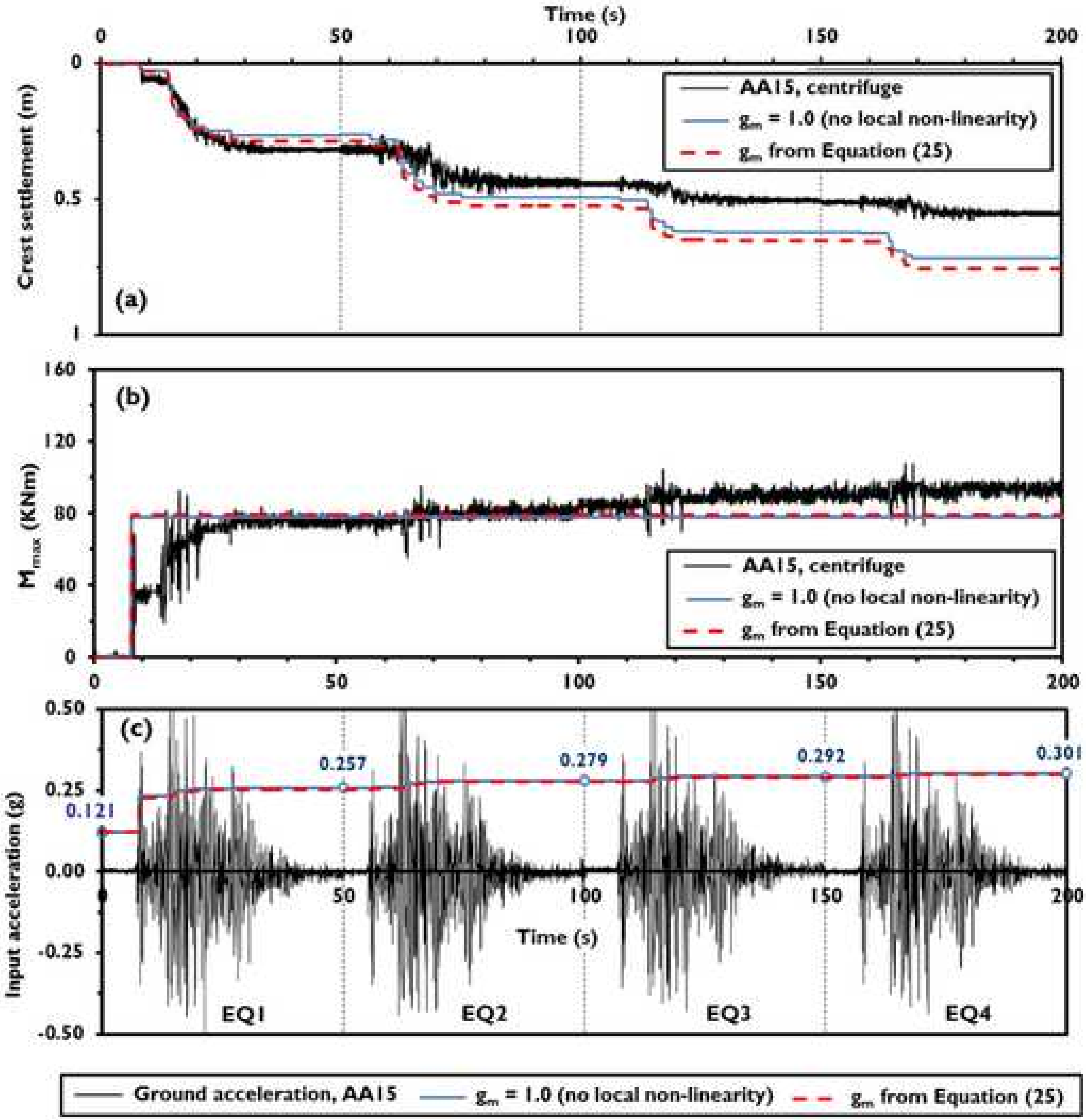

Figure 18
Click here to download high resolution image

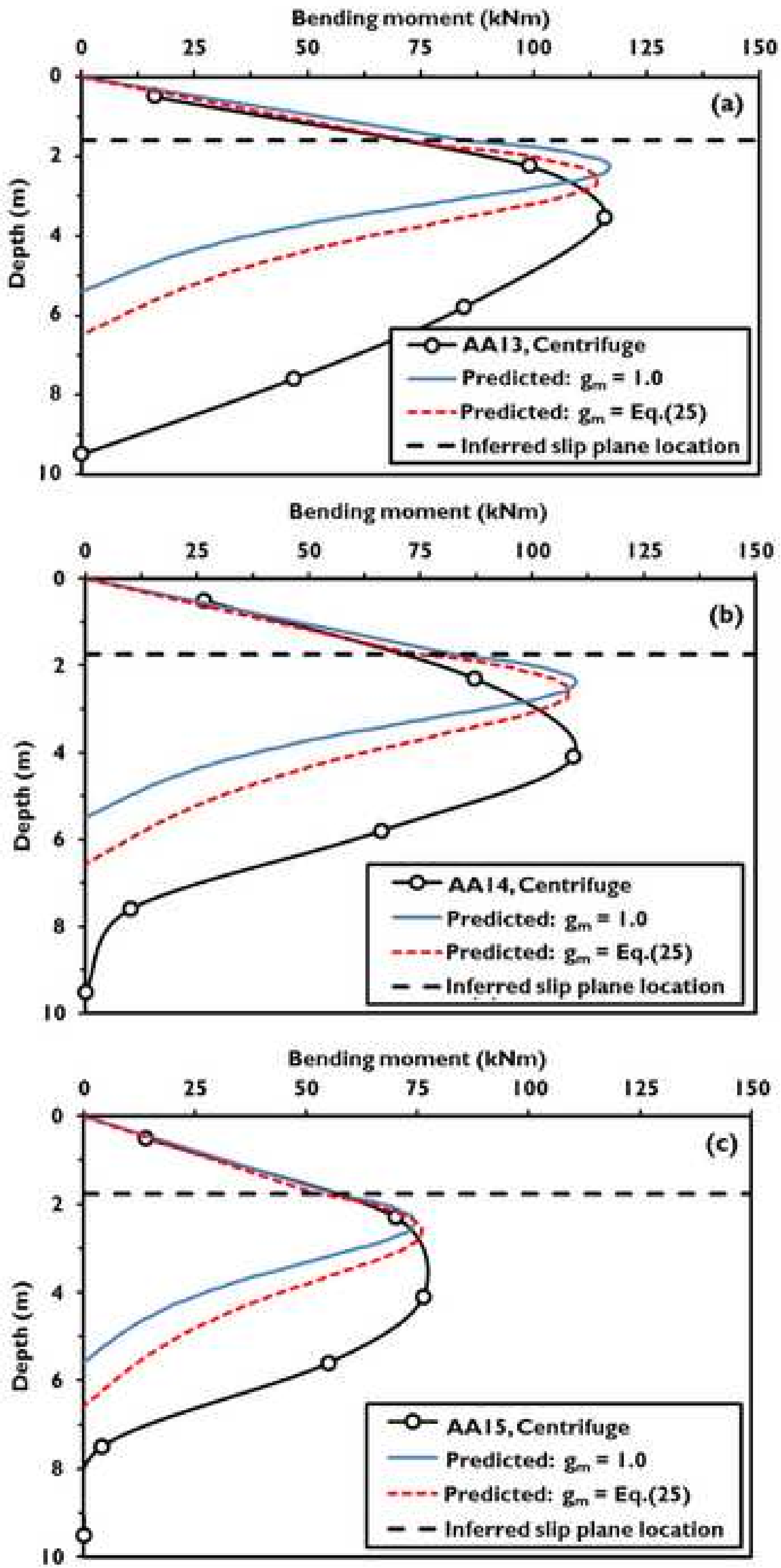

Figure 19
Click here to download high resolution image

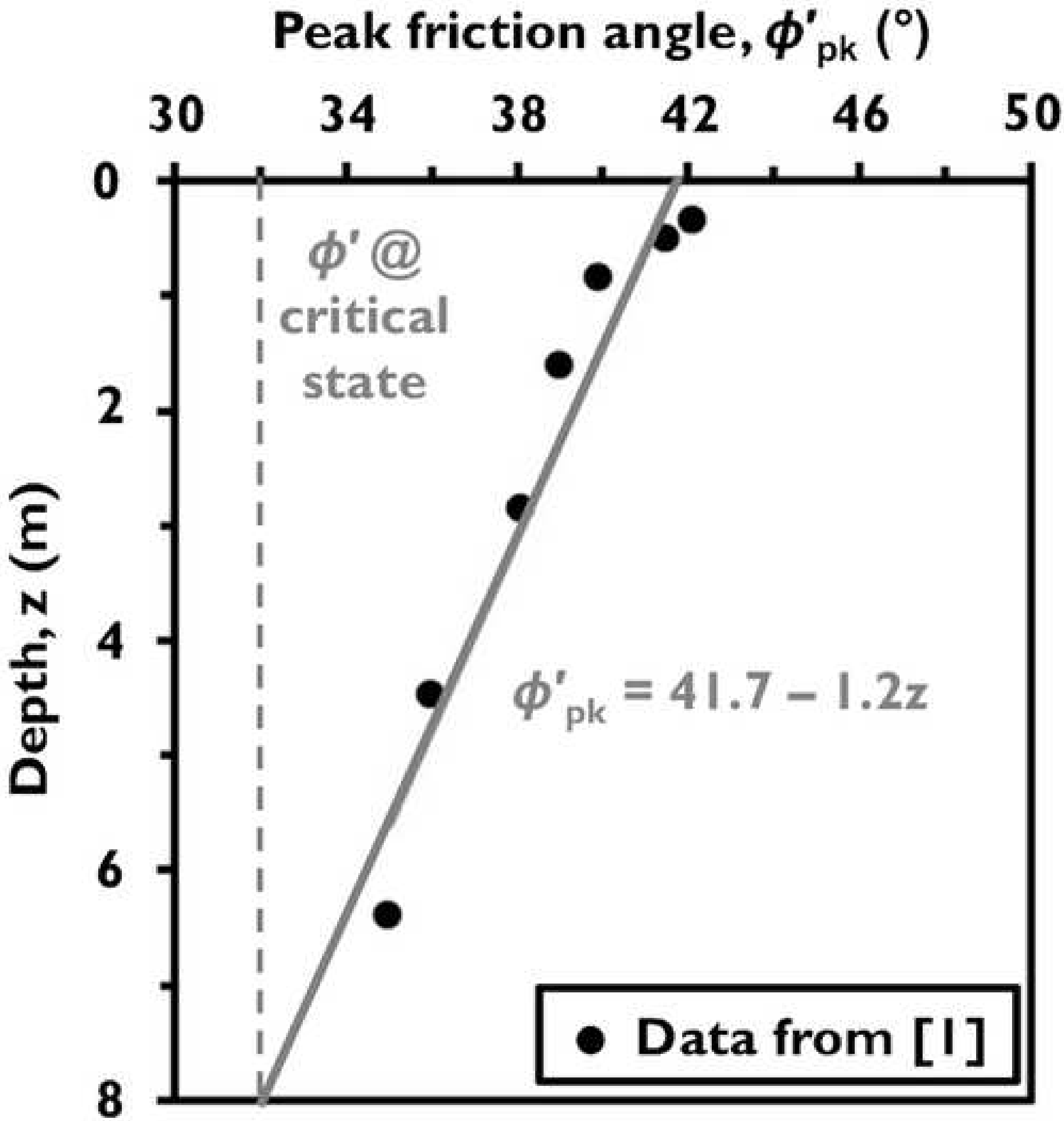

Figure 20
Click here to download high resolution image